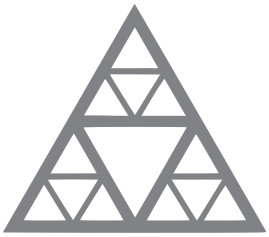

École des Ponts ParisTech

2021
Rapport de stage court

Zuodong WANG

Élévè ingénieur

Hybrid high-order method for elliptic PDEs on curved and complicated domains

(Méthode HHO pour les EDPs elliptiques sur domaines à frontière complexe)

Stage réalisé au sein de Centre Inria de Paris

2 Rue Simone IFF, 75012 Paris

du 07/06/2021 au 03/09/2021

Maître de stage : Monsieur Zhaonan DONG

Fiche de synthèse

- Type de stage : stage court

- Année : 2021

- Auteur (Nom, prénom) : WANG, Zuodong

- Formation 2ème année (IMI, GI, SEGF, etc.) : IMI

- Titre du rapport : Hybrid high-order method for elliptic PDEs on curved and complicated domains

- Titre en français (pour les titres en langue étrangère) : Méthode HHO pour les EDPs elliptiques sur domaines à frontière complexe

- Organisme d'accueil : Centre Inria de Paris

- Pays d'accueil : France

- Responsable de stage : Zhaonan DONG

- Mots-clés caractérisant votre rapport : EDPs elliptiques, HHO, estimation d'erreur a posteriori

Résumé

Ce rapport présente la méthode hybride d'ordre élevé (HHO) pour l'équation de Poisson et l'équation de réaction et de diffusion singulièrement perturbée dans les domaines avec frontière rectangulaire, frontière courbe et frontière complexe. Les méthodes HHO d'ordre égal, HHO d'ordre mixte et HHO-Nistche sont introduites, l'analyse théorique est réalisée pour le cas le plus général, la méthode HHO-Nistche. Les deux autres méthodes sont brièvement mentionnées. Les performances numériques de ces méthodes sont étudiées et comparées théoriquement et numériquement. Pour les deux équations, l'analyse théorique de la stabilité, de la condition d'être bien posé, de la consistance et de l'estimation de l'erreur d'énergie est détaillée, et les expériences numériques réalisées dans ce rapport confirment les résultats de l'analyse théorique. De plus, l'analyse théorique de l'estimation de l'erreur L^2 et des applications aux frontières courbes et complexes pour le problème de Possion avec la condition limite mixte est détaillée par la première fois dans la littérature pour la méthode HHO-Nistche.

Abstract

This report introduces the hybrid high-order (HHO) method for the Poisson equation and the singular-perturbed reaction diffusion equation posed in a domain with rectangular boundary, curved boundary and the complex boundary. The equal-order HHO method, the mixed-order HHO method and the HHO method employing the Nistche's boundary penalty techniques (HHO-N) are introduced. The detailed theoretical analysis is presented for the most general case, the HHO-N method. The other two methods are briefly mentioned. The numerical performance of these numerical methods are studied and compared theoretically and numerically. For the Possion problem and the singular-perturbed reaction diffusion problem, the theoretical analysis of the stability, well-posedness, consistency and energy error estimate is detailed, and the relevant numerical experiments realised in this report confirm the results of the theoretical analysis. Moreover, the theoretical analysis of the L^2 error estimate and the applications to curved and complex boundary for Possion problem with mixed boundary condition is detailed for the first time in the literature for HHO-N method.

Synthèse du rapport en français

Le stage traite d'une méthode numérique de résolution d'équation aux dérivées partielles appelée HHO (hybride high order). Le but du stage est de comprendre et maîtriser le concept de cette méthode qui a été proposée récemment, le processus d'analyse théorique et les avantages et inconvénients de cette méthode sur les calculs numériques. L'ensemble du stage est divisé en cinq parties. La première partie est l'apprentissage et la compréhension de base de la méthode HHO. La deuxième partie est de réaliser l'algorithme HHO de l'équation de Poisson au niveau numérique et de programmer des exemples précis sur les domaines simples. La troisième partie consiste à apprendre la théorie de la méthode de Nistche, et à utiliser cette méthode pour construire et résoudre des problèmes de Poisson posé sur des domaines avec des frontières complexes. La quatrième partie consiste à mettre en œuvre la méthode au niveau numérique et à donner des exemples numériques précis sur les domaines complexes. La cinquième partie consiste à étudier l'équation de réaction-diffusion linéaire qui est proche du problème de Poisson. À nouveau, une analyse détaillée est donnée à la fois numériquement et théoriquement.

La première étape du stage est principalement basée sur la lecture de la littérature, qui comprend la lecture de la théorie des éléments finis, l'analyse fondamentale du problème de Poisson, l'introduction de la méthode HHO et la réalisation de la méthode HHO pour le problème de Poisson. Plus précisément, la littérature sur la méthode des éléments finis du problème de Poisson se concentre principalement sur la discussion de la régularité de la solution sous différentes conditions aux limites et la réalisation du problème de Poisson par la méthode des éléments finis. Ceci est également entrecoupé avec la programmation par éléments finis du problème de Poisson. Bien que j'ai suivi quelques cours connexes à l'école, afin de résoudre des problèmes avec des frontières complexes plus tard, à ce stade, j'ai quand même réappris la réalisation de la programmation par éléments finis dans l'espace à deux dimensions, y compris le module 'distmesh' pour générer un maillage que je n'avais pas appris dans ma formation à l'Ecole des Ponts. La littérature de la méthode HHO que j'ai lue se concentre principalement sur la résolution du problème de Poisson, la méthode d'ordre égal et la méthode d'ordre mixte étant les principales. (Voir mon rapport pour les définitions concrètes). Cela comprend l'étude du concept de construction et du processus de la méthode numérique, et l'étude au niveau théorique comprend l'étude de la stabilité et de la convergence de la méthode. Parce que la tâche principale est uniquement d'apprendre et de reproduire les résultats numériques existants et l'analyse théorique, l'apprentissage à ce stade s'est déroulé sans obstacles, et les tâches associées se sont terminées avec succès dans le temps imparti.

Dans la deuxième partie, la tâche de programmation de la méthode HHO s'est avérée légèrement plus difficile. Comme je n'y avais pas d'expérience de programmation suffisante pour les problèmes d'équations différentielles bidimensionnelles, il a fallu un peu de temps pour m'adapter et apprendre des idées de programmation de base et des compétences de débogage lors du démarrage. Plus précisément, lorsque j'ai commencé à programmer, j'espérais mettre en œuvre la méthode HHO avec une petite quantité de modifications à

partir d'un autre programme d'éléments finis, mais ce processus n'était pas facile. Après avoir essayé pendant une semaine sans succès, avec l'aide de mon tuteur, j'ai réalisé le programme d'ordre égal de HHO pour résoudre l'équation de Poisson de la condition limite de Dirichlet sur un domaine rectangulaire. Ensuite, j'ai implémenté la méthode HHO d'ordre mixte pour ce problème basé sur le programme de HHO d'ordre égal avec un peu de modification. Ensuite, il a fallu quelques jours pour implémenter le problème de Poisson avec des conditions aux limites mixtes. Dans ce processus, j'ai acquis beaucoup de compétences en débogage. Par exemple, je peux utiliser différentes fonctions de test pour détecter si le bug apparaît sur la frontière, si le bug apparaît sur la structure d'une certaine matrice ou l'erreur de calcul.

La troisième partie concerne l'étude théorique de la méthode HHO-Nistche. Cette partie a été beaucoup plus difficile que les précédentes, car les références considèrent un problème de Poisson couplé, pas le problème de Poisson uniquement défini sur une seule région connectée que je considérais dans mon stage. J'ai dû d'abord apprendre la méthode HHO-Nitsche à partir de la littérature, puis l'appliquer aux problèmes à considérer dans mon stage. Par conséquent, j'ai dû d'abord bien maîtriser les idées de la littérature, puis modifier une partie de la théorie pour l'adapter au problème que je voulais traiter. Bien qu'il y ait eu un léger contretemps au milieu, j'ai également terminé cette partie de l'étude dans les délais prévus.

La quatrième partie concerne la réalisation numérique de la méthode HHO-Nistche. Les difficultés de cette partie se traduisent principalement en deux points. Tout d'abord, j'ai dû modifier l'opérateur de la méthode HHO d'origine. Comme la méthode HHO-Nistche a été modifiée sur certains éléments de bord, j'ai eu besoin de changer une partie de l'arrangement des variables du programme d'origine. Ensuite, ces modifications mineures ont entraîné des changements dans le niveau de calcul numérique. Par conséquent, j'ai dû également modifier certaines méthodes de calcul de l'opérateur. La partie la plus difficile de la programmation HHO pour moi a été de trouver l'ordre de la cellule et l'ordre de la variable, j'ai donc passé beaucoup de temps à écrire un certain nombre de programmes pour trouver l'ordre pertinent. Deuxièmement, j'ai dû étendre la méthode à des frontières complexes. Bien que les éléments internes soient des triangles ou des polygones généraux et que leurs côtés soient des lignes droites, le code existant peut approximer et calculer les fonctions sur les éléments internes très efficacement, mais sur la frontière, comme nous devons introduire des bords courbes, les calculs généraux doivent être adaptés. J'ai donc passé du temps à réfléchir à la façon de traiter les bords courbes. Il existe deux méthodes de traitement principales. L'une consiste à créer une transformation non-linéaire d'un bord courbe à un bord rectiligne. Son avantage est qu'elle peut être appliqué à la plupart des bords courbes. Cependant, cette solution nécessite la matrice Jacobienne de la transformation. Pour déterminer la transformation, de nombreuses itérations sont nécessaires, si bien que l'efficacité du calcul n'est pas très bonne. La deuxième méthode consiste à approcher le bord courbe par de nombreuses lignes droites. Cette méthode est très simple à mettre en œuvre et l'efficacité du calcul est élevée. J'ai donc finalement choisi et mis en œuvre cette idée.

Avant de passer à la cinquième partie, j'ai constaté que personne n'avait réalisé l'estimation de l'erreur L^2 de la méthode HHO-Nitsche avec des conditions aux limites mixtes. Donc mon tuteur et moi avons essayé cela et avons trouvé un résultat intéressant et ori-

ginal en deux à trois semaines. Bien qu'il y ait eu une preuve théorique du problème avec conditions aux limites de Dirichlet, lorsque nous avons essayé de l'étendre aux conditions aux limites mixtes, nous avons rencontré de nombreuses difficultés inattendues. Ces difficultés provenaient des calculs théoriques lourds induits par la méthode HHO d'une part, et d'autre part des différences subtiles de conception d'algorithmes entre le problème de Dirichlet et le problème aux frontières mixtes. Afin de surmonter ces difficultés, nous avons essayé de nombreuses idées. La grande différence entre la méthode HHO et les autres méthodes est, pour la plupart des méthodes d'éléments finis, si elles ont l'estimation d'erreur H^1, l'estimation d'erreur L^2 peut être facilement trouvée à travers un problème dual. Pour HHO, bien que nous considérons également le problème dual, la complexité des calculs théoriques est considérablement augmentée.

Puis comme il restait environ un mois pour le stage, j'ai entrepris de résoudre l'équation de réaction et diffusion linéaire. La différence entre cette équation et le problème de Poisson est la suivant : lorsque le coefficient de diffusion est dominant, on obtient essentiellement un problème de Poisson classique, alors que le coefficient de diffusion est faible, on obtient une équation algébrique. Par conséquent, nous devons ajuster la méthode HHO afin qu'elle puisse passer continûment d'une méthode de résolution d'équations aux dérivées partielles à une méthode de résolution d'équations algébriques. Cela implique l'introduction d'un nouvel espace de fonctions, la définition de divers opérateurs dans le nouvel espace de fonctions et la compatibilité des méthodes numériques. Heureusement, certains mathématiciens ont donné des résultats qui peuvent être utilisés comme référence sur d'autres problèmes similaires. Par conséquent, nous avons appris leurs méthodes et défini une méthode HHO qui est applicable à l'équation de réaction-diffusion et peut gérer des conditions aux limites complexes. Ensuite, nous avons effectué une analyse théorique de la méthode, de la stabilité et de l'ordre de convergence, et donné une série d'exemples numériques.

Au cours de ce stage, mes capacités en mathématiques et en programmation se sont considérablement améliorées. Tout d'abord, après ces trois mois de formation, ma compréhension des équations aux dérivées partielles elliptiques linéaires s'est considérablement accrue. Par exemple, j'ai une compréhension plus profonde de la régularité de la solution, et de l'influence de la régularité de la solution sur la performance de la méthode numérique, sur l'influence des conditions aux limites sur la régularité de la solution, etc. En outre, ma compréhension des méthodes numériques a également fait de grandes avancées, telles que les limitations de la méthode des éléments finis continus, les avantages de la méthode des éléments finis discontinus par rapport à celle-ci, et les excellentes performances des méthodes hybrides dans les solutions numériques. Deuxièmement, après trois mois de formation, je me suis fondamentalement familiarisé avec le processus d'analyse théorique de la méthode HHO et la méthode générale des éléments finis et l'utilisation des outils mathématiques fondamentaux. L'étude de la méthode de Nitsche a renforcé ma compréhension du concept de 'faiblement imposé', tandis que l'étude de l'équation de réaction-diffusion m'a aidé à comprendre concrètement les avantages de la méthode de Nitsche pour traiter de tels problèmes.

L'ensemble du stage s'est essentiellement déroulé selon le plan initial. Beaucoup de temps a été consacré à certaines expériences numériques et à plusieurs points d'analyse théorique plus difficiles. La partie la plus ardue du stage a été le débogage. En effet,

chaque exemple numérique a nécessité deux ou trois jours de débogage. Le fruit de mes efforts est que mes capacités de programmation ont été considérablement améliorées.

En raison de l'épidémie, j'avais pu librement choisir de travailler à distance pendant le stage. Mais il m'a été possible de travailler en présentiel et de rencontrer librement mon tuteur. Ainsi, l'efficacité de l'ensemble du stage a été très élevée.

En termes de langue, la communication avec les collègues de l'institut est essentiellement l'anglais et le français, donc ma maîtrise des langues étrangères s'est également améliorée dans une certaine mesure.

J'ai découvert de nombreux domaines de recherche auprès de mes collègues d'Inria, qui incluent non seulement les mathématiques fondamentales et les mathématiques appliquées, mais aussi beaucoup de connaissances en finance et en informatique. Ces connaissances provenant de différentes directions ont enrichi ma culture et approfondi ma compréhension des mathématiques sous différents angles. Ces connaissances m'ont également aidé à choisir le travail que je veux faire à l'avenir et le domaine dans lequel j'espère m'engager. J'espère m'engager dans la recherche sur les équations aux dérivées partielles dans le futur et ce stage m'en a donné l'envie. Durant la période d'Inria, j'ai senti que ma compréhension des équations aux dérivées partielles s'était significativement améliorée par rapport à avant, et la discussion avec mes collègues en optimisation convexe, finance, probabilités m'a également permis de mieux comprendre le cadre des mathématiques, et j'ai souvent l'impression que tous les domaines sont interopérables et que les méthodes de recherche et les compétences théoriques dans de nombreux domaines peuvent être utilisées dans d'autres domaines.

Dans ce stage, j'ai réalisé des progrès significatifs à la fois dans la théorie mathématique et dans mes capacités de programmation. Je remercie sincèrement mon tuteur DONG Zhaonan pour ses conseils et son aide précise au cours de ces trois mois. DONG Zhaonan a beaucoup investi de son énergie et de son temps tout au long de mon stage, de la sélection du contenu du stage à chaque détail des mathématiques et de la programmation, il m'a patiemment aidé et a répondu à toutes mes questions, même si ma question était parfois naïve. Je suis très honoré et chanceux d'avoir pu accepter ses conseils pendant ces trois courts mois !

Par ailleurs, je remercie le Professeur Alexandre ERN de m'avoir recommandé pour un stage à cet institut de recherche de renommée mondiale, l'Inria. J'aime beaucoup cet institut grâce à l'ambiance conviviale des collègues et l'ambiance académique libre qui m'attire profondément. Au passage, le climatiseur de l'INRIA m'a motivé à travailler ici tous les jours au lieu de travailler en distanciel.

Acknowledgements

In this internship, I have achieved significant improvement in both mathematical theory and programming ability. I sincerely thank my intern tutor Dong Zhaonan for his step-by-step guidance and help during these three months. DONG Zhaonan invested a lot of his energy and time in my entire internship, from the selection of the content of the internship to every detail of mathematics and programming. He patiently helped me and answered all my questions no matter how naive my question could be. I am very honored and lucky to have been able to receive his guidance during this short three months!

In addition, I am grateful to Prof. Alexandre Ern for recommending me to this world-leading research institute, INRIA for an internship. I really like this institute because of the friendly atmosphere of colleagues and the free academic atmosphere which deeply attracts me. By the way, the air conditioner in INRIA motivated me to work here everyday instead of remote work!

Wang Zuodong,
Paris,
August, 2021.

Table des matières

Liste des tableaux

Table des figures

1. Introduction

This internship project is designed for studying the theory and practical implementation of the recently developed Hybrid High-Order methods (HHO). In particular, we will focus on the numerical approximation of the HHO methods employing the Nitsche's technique (HHO-N) for solving the Poisson problems on the domains with complicated boundary. The HHO-N method supports arbitrary order approximation on general shaped elements employing polygonal elements with a possibly arbitrary number of faces. We prove that the HHO-N method's stability and convergence rate are independent of the number and measure of $(d-1)$-dimensional faces on the domain boundary under very mild mesh assumptions. Moreover, a series of numerical examples are presented to confirm the theory in this report.

Hybrid high-order (HHO) methods use discrete unknowns to the cells and to the faces of the mesh. The core of their design is two intuitive ideas : (i) a local operator reconstructing in every mesh cell for approximating the continuous operator (like the gradient operator) from the local cell and face unknowns and (ii) a local stabilization operator for dealing with the kernel issue of the reconstruction operator. These two local operators are then combined into a local discrete bilinear form, and the global problem is assembled cell-wise as in standard finite element methods. HHO methods offer many attractive features : support of polyhedral meshes, optimal convergence rates, a dimension-independent formulation, and robustness in various regimes (e.g., no volume-locking in linear elasticity). Moreover, their computational efficiency hinges on the possibility of locally eliminating the cell unknowns by static condensation, leading to a global transmission problem coupling only the face unknowns.

HHO methods were introduced in [18, 20] for linear diffusion and quasi-incompressible linear elasticity. A high-order method in mixed form sharing the same devising principles was introduced in [19], and shown in [2] to lead after hybridization to a HHO method with a slightly different, yet equivalent, writing of the stabilization. The realm of applications of

HHO methods has been substantially expanded over the last few years. Developments in solid mechanics include elasticty [5], plasticity [1], Kirchhoff–Love plates [3], obstacle [13], two-membrane contact problems [15], acoustic and elastic wave propagation [7]. Those related to fluid mechanics include convection-diffusion in various regimes [16], Stokes [21], Navier–Stokes [22], etc.

The goal of the present work is to devise, analyze theoretically and evaluate numerically a HHO-Nitsche method to the Possion equation and the reaction diffusion equation. The devising and analysis of HHO-Nitsche methods started in [11] for the scalar Signorini problem. Nitsche's method was created to weakly enforce the jump conditions at the interface or the Dirichlet conditions at the domain boundary. We refer the reader, e.g., to [6, 9] for further advances and overviews on the topic. In this report, we extend the Nistche's method in two directions : Firstly, we apply it in the mixed boundary condition of Dirichlet boundary condition and Neumann boundary condition, secondly, we apply it in the complex boundary, i.e., the boundary was composed by many small edges. Another novelty of this report is the L^2 error estimate for the Possion equation on the mixed boundary condition. Moreover, a lot of numerical experiments are realized and discussed in this report, these experiments present the advantages of HHO methods in different aspects.

This report is organized as follows : Chapter 2 presents the notations, discrete settings and the model of the Possion problem. The HHO methods will be detailed in chapter 3. In chapter 4, the theoretical analysis of the Possion problem is studied. The implementation aspects and programming techniques are discussed in chapter 5. A lot of numerical experiments in chapter 6 confirm the theoretical analysis in chapter 4 and the the influences of programming techniques in chapter 5. In chapter 7, the reaction diffusion equation is briefly studied. Finally, the chapter 8 is devoted to the conclusion and personal review.

2. Model and Notations

In this chapter, we present the model, and in the report, we follow the standard notations in Sobolev space, $\|\cdot\|$ means standard L^2 norm and $|\cdot|_{H^{t+1}}$ means standard H^{t+1} seminorm, and we simplify the notation of L^2 inner product as $(\cdot,\cdot)$, if there is no special statement.

2.1. Model Problem

Let Ω be a open, Lipschitz and connected domain in $\mathbb{R}^d, d \in \{2,3\}$, $\Gamma = \Gamma_D \cup \Gamma_N$, where Γ_D is the closed Dirichlet boundary satisfying $|\Gamma_D| > 0$ and Γ_N is the Neumann boundary. We consider the solution $u \in H^1(\Omega)$ of the following elliptic boundary problem :

$$-\Delta u = f \qquad \text{in} \quad \Omega, \tag{2.1}$$

$$u = g_D \qquad \text{on} \quad \Gamma_D, \tag{2.2}$$

$$\nabla u \cdot \boldsymbol{n} = g_N \qquad \text{on} \quad \Gamma_N, \tag{2.3}$$

with $f \in L^2(\Omega), g_D \in H^{\frac{1}{2}}(\Gamma_D)$ and $g_N \in L^2(\Gamma_N)$.

The weak form of the above problem is defined as : Find $u \in H^1(\Omega)$, satisfying $u|_{\Gamma_D} = g_D$ and $\nabla u \cdot \boldsymbol{n}|_{\Gamma_N} = g_N$,

$$a(u,v) = \ell(v), \qquad \forall v \in H^1_{\Gamma_D}(\Omega), \tag{2.4}$$

with $a(u,v) := (\nabla u, \nabla v)_\Omega$ and $\ell(v) := (f,v)_\Omega + (g_N, v)_{\Gamma_N}$, where $H^1_{\Gamma_D}(\Omega) = \{v \in H^1(\Omega) | v = 0 \text{ on } \Gamma_D\}$.

2.2. Polytopal and curved meshes

Let $\{\mathcal{T}_h\}_{h>0}$ be a mesh family such that each mesh $\mathcal{T}_h$ covers Ω exactly. A generic mesh cell is denoted by $T \in \mathcal{T}_h$, its diameter by h_T, and its unit outward normal by $\boldsymbol{n}_T$. We partition the boundary ∂T of any mesh cell $T \in \mathcal{T}_h$ by means of the two subsets $\partial T^i := \partial T \cap \overline{\Omega}$, $\partial T^b := \partial T \cap \partial\Omega$. Similarly, we partition the mesh as $\mathcal{T}_h = \mathcal{T}_h^i \cup \mathcal{T}_h^b$, where $\mathcal{T}_h^i$

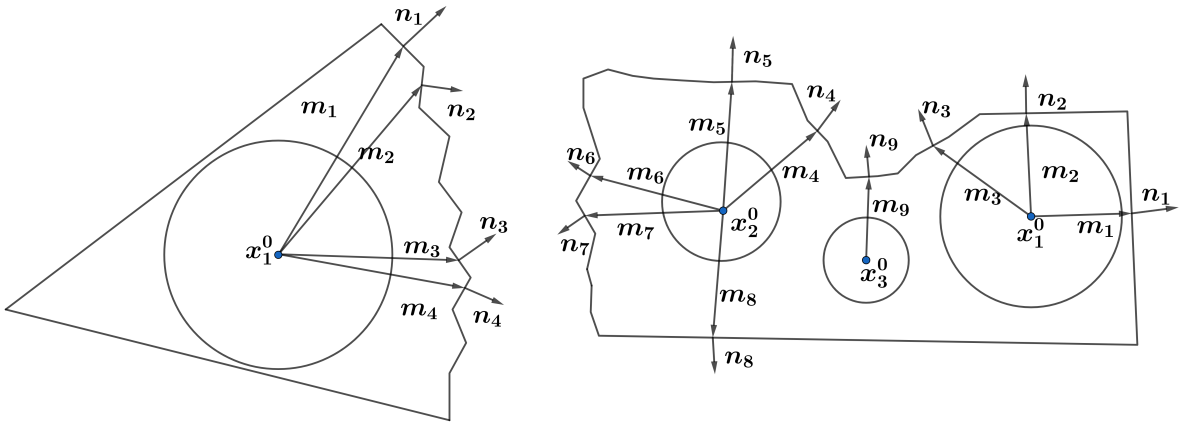

FIGURE 2.1 – Examples for mesh assumption

is the collection of all the mesh cells T such that ∂T^b has positive measure. Moreover, we further split ∂T^b into two nonoverlapping subsets $\partial T^D := \partial T^b \cap \Gamma_D$ and $\partial T^N := \partial T^b \cap \Gamma_N$. The mesh faces are collected in the set $\mathcal{F}_h$, which is split as $\mathcal{F}_h = \mathcal{F}_h^i \cup \mathcal{F}_h^b$, where $\mathcal{F}_h^i$ is the collection of the interior faces (shared by two distinct mesh cells) and $\mathcal{F}_h^b$ the collection of the boundary faces. For all $F \in \mathcal{F}_h$, we orient F by means of the fixed unit normal vector $\boldsymbol{n}_F$ whose direction is arbitrary for all $F \in \mathcal{F}_h^i$ and $\boldsymbol{n}_F := \boldsymbol{n}_\Omega$ for all $F \in \mathcal{F}_h^b$. For any mesh cell $T \in \mathcal{T}_h$, the mesh faces composing its boundary ∂T are collected in the set $\mathcal{F}_{\partial T}$, which is partitioned as $\mathcal{F}_{\partial T} = \mathcal{F}_{\partial T^i} \cup \mathcal{F}_{\partial T^D} \cup \mathcal{F}_{\partial T^N}$ with obvious notation.

Assumption 2.1. *(1). The interior mesh $\mathcal{T}_h^i$ is assumed to be shape-regular polyhedral mesh sequences, i.e., for all $h > 0$, $\mathcal{T}_h$ admits a matching submesh $\mathcal{T}_h'$ such that any cell (or face) of $\mathcal{T}_h'$ is a cell (or face) of $\mathcal{T}_h$. Moreover, there exists a mesh-regularity parameter $\rho > 0$ such that for all $h > 0$, all $T \in \mathcal{T}_h$ and all $S \in \mathcal{T}_h'$ such that $S \subset T$, we have $\rho h_S \leq r_S$ and $\rho h_T \leq h_S$, where r_S denotes the inradius of the polytope S.*

(2). For any boundary mesh cell $T \in \mathcal{T}_h^b$, all the face in $\mathcal{F}_{\partial T^i}$ are planar with diameter uniformly equivalent to h_T. Moreover, for each ∂T^b, T can be decomposed into a finite union of nonoverlapping subsets, $T = \{T_{\partial T^b,m}\}_{m\in\{1,\dots,n_{T,\partial T^b}\}}$, such that $T_{\partial T^b,m}$ is star-shaped with respect to an interior ball of radius $r_{T,m}$ satisfying $\rho h_T \leq r_{T,m}$, with the mesh-regularity parameter $\rho > 0$. See Figure 2.1 for an illustration with $n_{T,\partial T^i} = 1$ (left) and $n_{T,\partial T^i} = 3$ (right).

Remark 2.1 (Mesh assumptions). *The above mesh assumptions on the mesh sequence are fairly general. Let us briefly discuss some of the most significant ones. (1) The assumption that the interior faces of the mesh are planar is important in the present setting of HHO methods which use polynomial functions as discrete unknowns attached to these interior faces. Notice though that the use of a Nitsche-like penalty method allows us to avoid introducing discrete unknowns on the boundary faces; thus, such faces do not need to be planar. (2) The star-shapedness assumption on the mesh boundary cells is introduced to invoke a Poincaré-type inequality in such cells. Moreover, the mesh assumption of the boundary cells allows the smoothed curved faces and arbitrary number of faces with arbitrary small measure.*

2.3. Analysis tools

Let us briefly review the main analysis tools used in this report. We only state the results and refer to Remark 2.2 for some comments on the proofs. In what follows, we always consider a shape-regular mesh sequence satisfying Assumption 2.1. Moreover, in various bounds, we use $a \lesssim b$ to denote $a \leq Cb$ with C to be any generic constant (its value can change at each occurrence) that is independent of mesh size $h > 0$, but may depend on the shape-regularity of the mesh sequence and the polynomial degree for all $T \in \mathcal{T}_h$.

Lemma 2.1 (Discrete trace inequalities). *Let $k \in \mathbb{N}$ be the polynomial degree and let element $T \in \mathcal{T}_h$, and $v_T \in \mathbb{P}_{k,d}(T)$. Then, the following discrete inequalities hold true :*

$$\|v_T\|_{\partial T} \lesssim h_T^{-\frac{1}{2}} \|v_T\|_T. \tag{2.5}$$

Lemma 2.2 (Multiplicative trace inequality). *Let element $T \in \mathcal{T}_h$. Then, the following statement holds true for all $v \in H^1(\Omega)$:*

$$\|v\|_{\partial T} \lesssim (h_T^{-\frac{1}{2}} \|v\|_T + \|v\|_T^{\frac{1}{2}} \|\nabla v\|_T^{\frac{1}{2}}). \tag{2.6}$$

Lemma 2.3 (Polynomial approximation). *Let $k \geq 0$ be the polynomial degree, and there*

is a real number $t \in [0, k+1]$*, all* $m \in \{0, \ldots, \lfloor t \rfloor\}$*, all* $h \geq 0$*, and* $u \in H^{t+1}(T)$*,*

$$|v - \Pi_T^k(v)|_{H^m(T)} \lesssim h_T^{t-m} |v|_{H^t(T)}, \tag{2.7}$$

where Π_T^k *denoted the* L^2*-orthognal projection onto* $\mathbb{P}_{k,d}(T)$*.*

Let us briefly highlight some useful consequences of the above results. From the (2.7), the classical Poincaré inequality holds by taking $k = 0$, $m = 0$ and $t = 1$: For all $T \in \mathcal{T}_h$,

$$\|v - \Pi_T^0 v\|_T \lesssim h_T \|\nabla v\|_T, \qquad \forall v \in H^1(T). \tag{2.8}$$

The following consequences of (2.8) combined with the multiplicative trace inequality (2.6) will be useful in our analysis : Letting $k \geq 0$ be the polynomial degree we have for all $v \in H^{t+1}(T)$,

$$\begin{aligned} \|v - \Pi_T^{k+1}(v)\|_T + h_T^{\frac{1}{2}} \|v - \Pi_T^{k+1}(v)\|_{\partial T} + h_T \|\nabla(v - \Pi_T^{k+1}(v))\|_T \\ + h_T^{\frac{3}{2}} \|\nabla(v - \Pi_T^{k+1}(v))\|_{\partial T} \lesssim h_T^{t+1} |v|_{H^{t+1}(T)}. \end{aligned} \tag{2.9}$$

Remark 2.2. *We briefly comment on the proofs of the above lemmas. For the Lemma 2.1 and Lemma 2.2, the proof on mesh cells having flat faces can be found in [17, Sec. 1.4.3]. On the mesh cells having a curved face, these results can be found in [8, 29] assuming that the curved face is a* C^2 *manifold. More recently, these results were extended in [10] with fully explicit constants to Lipschitz manifolds satisfying the mild additional geometric assumptions.*

Concerning Lemma 2.3, the key step is to establish the Poincaré inequality (2.8) *since* (2.7) *can then be derived by using recursively the Poincaré inequality. On the interior mesh cells, which can be decomposed as a finite union of (convex) subsimplices, this latter inequality is established by proceeding as in [23, 28]. On the boundary mesh cells, which can have a curved face, one invokes the star-shapedness assumption with respect to a ball. We refer the reader to [30] for the derivation of this inequality with an explicitly determined constant under such an assumption.*

3. HHO Methods

In this chapter, we will present 3 different HHO methods : the equal-order HHO method, the mixed-order HHO method and HHO-N method. The equal-order HHO is the first version of HHO method, it employs the same order of polynomial bases functions for cell unknowns and face unknowns. The mixed-order HHO is a variant of equal order case, which employs polynomial bases with one order in the cell unknowns compare to the polynomial bases on the face unknowns. Both of the above two HHO methods are not able to handle complicated/curved boundaries in an efficient way, so we will only consider the simple shape-regular polytopal meshes for the above two HHO methods. Finally, we introduce the mixed order HHO method employing the Nistche's (HHO-N) boundary penalty technique to deal with the complicated/curved boundary conditions.

3.1. The equal-order HHO method

Let $k \geq 0$ be the polynomial degree. We consider a pair $\hat{v}_T := (v_T^k, v_{\partial T}^k)$, where v_T^k is defined on T and $v_{\partial T}^k$ is defined on the faces (facewise) $F \in \mathcal{F}_{\partial T}$ composing the boundary ∂T of T. We define the local HHO space

$$\hat{V}_T := \mathbb{P}_{k,d}(T) \times \mathbb{P}_{k,d-1}(\mathcal{F}_{\partial T}).$$

An element $\hat{v}_T \in \hat{V}_T$ is denoted $\hat{v}_T := (v_T^k, v_{\partial T}^k)$, with $v_T^k \in \mathbb{P}_{k,d}(T)$ and $v_{\partial T}^k \in \mathbb{P}_{k,d-1}(\mathcal{F}_{\partial T})$. The first component of $\hat{v}_T$ aims at representing the solution inside the mesh cell, and the second component is representing the trace. Moreover, we have $\dim(\mathbb{P}_{k,d}) = \binom{k+d}{d}$, $\dim(\mathbb{P}_{k,d-1}) = \binom{k+d-1}{d-1}$, and $\dim(\hat{V}_T^k) = \binom{k+d}{d} + \sharp|\mathcal{F}_{\partial T}|\binom{k+d-1}{d-1}$.

We introduce a reconstruction operator $R_T : \hat{V}_T \to \mathbb{P}_{k+1,d}(T)$ using both cell unknowns and face unknowns s.t. for every pair $\hat{v}_T = (v_T^k, v_{\partial T}^k) \in \hat{V}_T$, the function $R_T(\hat{v}_T)$ is

s.t. for all $q \in \mathbb{P}_{k+1,d}(T)$,

$$(\nabla R_T(\hat{v}_T), \nabla q)_T := -(v_T^k, \Delta q)_T + (v_{\partial T}^k, \boldsymbol{n}_T \cdot \nabla q)_{\partial T} \tag{3.1}$$

$$= (\nabla v_T^k, \nabla q)_{L^2(T)} - (v_T^k - v_{\partial T}^k, \boldsymbol{n}_T \cdot \nabla q)_{\partial T}, \tag{3.2}$$

and $(R_T(\hat{v}_T) - v_T^k, 1)_{L^2(T)} := 0$. So $R_T(\hat{v}_T)$ can be regarded as a Neumann problem and its well-posedness is guaranteed by Lax-Milgram Lemma. In practice, we need to solve it by inverting the local stiffness matrix, see chapter 5 for more details.

Remark 3.1. In practice, (3.1) performs better than (3.2), although they are equivalent in mathematical level. This phenomenon will be analysed in chapter 5.

This reconstruction operator is not stable in practice since $\nabla R_T(\hat{v}_T) = 0$ does not imply that v_T^k and $v_{\partial T}^k$ are same constant functions taking the same value. We can prove it easily by a dimension argument : We have $\ker(R_T) \subset \{\hat{v}_T \in \hat{V}_T | \nabla R_T(\hat{v}_T) = 0\}$ and $\dim(\ker(R_T)) = \dim(\hat{V}_T) - \dim(\mathrm{im}(R_T)) \geq \dim(\hat{V}_T) - \dim(\mathbb{P}_{k,d}(T)) = \binom{k+d-1}{d-1}\frac{kd+1}{k+1} > 1$. In order to fix this problem, we can introduce a stabilization operator which is defined as an operator mapping $\hat{V}_T$ to face based functions $S_T : \hat{V}_T \to \mathbb{P}_{k,d-1}(\partial T)$ s.t. for all $\hat{v}_T \in \hat{V}_T$,

$$S_T(\hat{v}_T) := \Pi_{\partial T}^k(v_T^k - v_{\partial T}^k + (I - \Pi_T^k)R_T(\hat{v}_T)), \tag{3.3}$$

where I is identity and $\Pi_{\partial T}^k$ is the L^2-orthogonal projection to $\mathbb{P}_{k,d-1}(\partial T)$. This stabilization operator is considered for fixing the kernel issue.

With these two operators, we can define local bilinear form a_T^k in each cell T :

$$a_T^k(\hat{u}_T, \hat{v}_T) := (\nabla R_T(\hat{u}_T), \nabla R_T(\hat{v}_T))_T + h_T^{-1}(S_T(\hat{u}_T), S_T(\hat{v}_T))_{\partial T}, \tag{3.4}$$

for all $\hat{u}_T, \hat{v}_T \in \hat{V}_T$. Here we add the coefficient h_T^{-1} in the stabilization term for the optimal convergence.

Next, we define the global HHO space as

$$\hat{V}_h := \mathbb{P}_{k,d}(\mathcal{T}_h) \times \mathbb{P}_{k,d-1}(\mathcal{F}_h), \tag{3.5}$$

An element $\hat{v}_h \in \hat{V}_h$ is denoted $\hat{v}_h := (v^k_{\mathcal{T}_h}, v^k_{\mathcal{F}_h})$, with $v^k_{\mathcal{T}_h} := (v^k_T)_{T\in\mathcal{T}_h}$ and $v^k_{\mathcal{F}_h} = (v^k_F)_{F\in\mathcal{F}_h}$.

Then, we can define the global forms a_h and ℓ_h s.t.

$$a^k_h(\hat{u}_h, \hat{v}_h) = \sum_{T\in\mathcal{T}_h} a^k_T(\hat{u}_T, \hat{v}_T), \tag{3.6}$$

$$\ell^k_h(\hat{v}_h) = \sum_{T\in\mathcal{T}_h} \big((f, v^k_T)_T + (g_N, v^k_T)_{\partial T^N}\big), \tag{3.7}$$

for all $\hat{u}_h, \hat{v}_h \in \hat{V}_h$. The discrete problem thus is defined as follows :

$$\begin{cases} \text{Find } \hat{u}_h \in \hat{V}_h \text{ such that} \\ a^k_h(\hat{u}_h, \hat{v}_h) = \ell^k_h(\hat{v}_h),\ \forall \hat{v}_h \in \hat{V}_h. \end{cases} \tag{3.8}$$

Remark 3.2. *An important observation is that the discrete problem* (3.6) *can be solved by the the static condensation. Indeed, the cell unknowns can be eliminated locally in every mesh cell, leading to a global problem where the only remaining unknowns are those attached to the mesh faces in* $\mathbb{P}_{k,d-1}(\mathcal{F}^i_h \cup \mathcal{F}^N_h)$*. Because the Dirichlet boundary data is enforced to the face unknowns in* $\mathbb{P}_{k,d-1}(\mathcal{F}^D_h)$ *directly.*

3.2. The mixed-order HHO method

In this section, we define the mixed-order HHO methods. Let $k \geq 0$ be the polynomial degree. We consider a pair $\hat{v}^m_T := (v^{k+1}_T, v^k_{\partial T})$, where v^{k+1}_T is defined on T and $v^k_{\partial T}$ is defined on the faces (facewise) $F \in \mathcal{F}_{\partial T}$ composing the boundary ∂T of T. We define the local HHO space

$$\hat{V}^m_T := \mathbb{P}_{k+1,d}(T) \times \mathbb{P}_{k,d-1}(\mathcal{F}_{\partial T}).$$

Similar to the equal-order HHO mehtod, we need to define the reconstruction operator and the stabilization operator. For the reconstruction operator, we define a map $R^m_T : \hat{V}^m_T \to \mathbb{P}_{k+1,d}(T)$ s.t. for each pair $\hat{v}^m_T = (v^{k+1}_T, v^k_{\partial T}) \in \hat{V}^m_T$, the function $R^m_T(\hat{v}^m_T)$ is s.t. for all $q \in \mathbb{P}_{k+1,d}(T)$,

$$(\nabla R^m_T(\hat{v}^m_T), \nabla q)_T := -(v^{k+1}_T, \Delta q)_T + (v^k_{\partial T}, \boldsymbol{n}_T \cdot \nabla q)_{\partial T} \tag{3.9}$$

$$= (\nabla v^{k+1}_T, \nabla q)_T - (v^{k+1}_T - v^k_{\partial T}, \boldsymbol{n}_T \cdot \nabla q)_{\partial T}, \tag{3.10}$$

and $(R_T^m(\hat{v}_T^m) - v_T^{k+1}, 1)_T := 0$ as the same as the equal-order HHO.

For stabilization term, notice that $(I - \Pi_T^{k+1})R_T^m(\hat{v}_T^m)_{\partial T} = (\Pi_T^{k+1} - \Pi_T^{k+1})R_T^m(\hat{v}_T^m)_{\partial T} = 0$, the stabilization term (3.3) can be simplified to

$$S_T^m(\hat{v}_T^m) := \Pi_{\partial T}^k(v_T^{k+1} - v_{\partial T}^k), \tag{3.11}$$

which is named as Lehrenfeld-Schoberl stabilization operator, see [26] for more applications of this operator.

Next, we define the global HHO space as

$$\hat{V}_h^m := \mathbb{P}_{k+1,d}(\mathcal{T}_h) \times \mathbb{P}_{k,d-1}(\mathcal{F}_h). \tag{3.12}$$

The global bilinear form of the mixed-order HHO methods is same as the equal-order HHO method. The global bilinear form is defined by summing up the local bilinear form. Using the obivious notation, the discrete problem is defined as follows :

$$\begin{cases} \text{Find } \hat{u}_h^m \in \hat{V}_h^m \text{ such that} \\ a_h^m(\hat{u}_h^m, \hat{v}_h^m) = \ell_h^m(\hat{v}_h^m), \ \forall \hat{v}_h \in \hat{V}_h^m, \end{cases} \tag{3.13}$$

where

$$a_h^m(\hat{u}_h^m, \hat{v}_h^m) = \sum_{T \in \mathcal{T}_h} \big((\nabla R_T^m(\hat{u}_T^m), \nabla R_T^m(\hat{v}_T^m))_T + h_T^{-1}(S_T^m(\hat{u}_T^m), S_T^m(\hat{v}_T^m))_{\partial T} \big), \tag{3.14}$$

$$\ell_h^m(\hat{v}_h^m) = \sum_{T \in \mathcal{T}_h} \big((f, v_T^{k+1})_T + (g_N, v_T^{k+1})_{\partial T^N} \big). \tag{3.15}$$

Remark 3.3. *For the mixed-order HHO, the cell unknowns in $\mathbb{P}_{k+1,d}(T)$, which is one order higher than the polynomial bases of face unknowns. This modification has a few advantages comparing to the equal-order HHO method on the computational performance and the theoretical analysis, and this detail is presented in chapter 4 and 5. On the other hand, we can also set cell unknowns in $\mathbb{P}_{k-1,d}(T)$ for the mixed-order HHO method, see chapter 39 of [24] for more choices of the mixed-order HHO method.*

3.3. The HHO method with Nitsche's boundary penalty

In this section, we will introduce the mixed-order HHO method employing Nitsche's boundary penalty techniques (HHO-N) for dealing with the complicated/curved boundary. We first start to introduce the HHO space. Let $k \geq 0$ be the polynomial degree. We consider a pair $\hat{v}_T^i := (v_T^{k+1}, v_{\partial T^i}^k)$, where v_T^{k+1} is defined on T and $v_{\partial T}^k$ is defined on the faces (facewise) $F \in \mathcal{F}_{\partial T}$ composing the boundary ∂T^i of T. We define the local HHO space

$$\hat{V}_T^i := \mathbb{P}_{k+1,d}(T) \times \mathbb{P}_{k,d-1}(\mathcal{F}_{\partial T^i}),$$

noticing the above local HHO-N space does not contain face unknowns on the boundary of the domain.

Next, the construction of HHO-N method is similar to two previous sections, we start with the reconstruction operator and the stabilization operator. As the boundary face unknowns are ignored, we remove boundary face unknowns from R_T^m and S_T^m, so our operators are defined as follows : $R_T^i : \hat{V}_T^i \to \mathbb{P}_{k+1,d}(T)$ s.t. for every pair $\hat{v}_T^i = (v_T^{k+1}, v_{\partial T^i}^k) \in \hat{V}_T^i$, the function $R_T^i(\hat{v}_T^i)$ is s.t. for all $q \in \mathbb{P}_{k+1,d}(T)$,

$$\begin{aligned}(\nabla R_T^i(\hat{v}_T^i), \nabla q)_T &:= -(v_T^{k+1}, \Delta q)_T + (v_{\partial T^i}^k, \boldsymbol{n}_T \cdot \nabla q)_{\partial T^i} + (v_T^{k+1}, \boldsymbol{n}_T \cdot \nabla q)_{\partial T^N} \qquad (3.16)\\ &= (\nabla v_T^{k+1}, \nabla q)_T - (v_T^{k+1} - v_{\partial T^i}^k, \boldsymbol{n}_T \cdot \nabla q)_{\partial T^i} - (v_T^{k+1}, \boldsymbol{n}_T \cdot \nabla q)_{\partial T^D}, \qquad (3.17)\end{aligned}$$

and together with the condition $(R_T^i(\hat{v}_T^i) - v_T^{k+1}, 1)_T := 0$. In addition, we define the lifting operator such that $L_T^{k+1} : L^2(\partial T^D) \to \mathbb{P}_{k+1,d}(T)$ for all $T \in \mathcal{T}_h$ such that, for all $g_D \in L^2(\partial T^D)$ and all $q \in \mathbb{P}_{k+1,d}(T)$,

$$(\nabla L_T^{k+1}(g_D), \nabla q)_T := (g_D, \nabla q \cdot \boldsymbol{n}_{\Gamma_D})_{\partial T^D}, \qquad (3.18)$$

$$(L_T^{k+1}(g_D), 1)_T := 0. \qquad (3.19)$$

We point out that $L_T^{k+1}(g_D) := 0$ for all interior cell $T \in \mathcal{T}_h^i$.

For the interior face $F \in \mathcal{F}_{\partial T^i}$, the LS stabilization operators are defined as

$$S_T^i(\hat{v}_T^i) := \Pi_{\partial T^i}^k(v_T^{k+1} - v_{\partial T^i}^k). \tag{3.20}$$

For the Dirichlet face $F \in \mathcal{F}_{\partial T^D}$, the stabilization operators are defined as

$$S_T^D(\hat{v}_T^i) := v_T^{k+1}|_{\partial T^D}. \tag{3.21}$$

Then, the local bilinear form a_T^i in each cell T is defined as follow :

$$a_T^i(\hat{u}_T^i, \hat{v}_T^i) := (\nabla R_T^i(\hat{u}_T^i), \nabla R_T^i(\hat{v}_T^i))_T + h_T^{-1}(S_T^i(\hat{u}_T^i), S_T^i(\hat{v}_T^i))_{\partial T^i} + h_T^{-1}(u_T^{k+1}, v_T^{k+1})_{\partial T^D}. \tag{3.22}$$

Next, we can define the global forms a_h^i, s_h^i and ℓ_h^i as follows :

$$a_h^i(\hat{u}_h^i, \hat{v}_h^i) := \sum_{T \in \mathcal{T}_h} a_T^i(\hat{u}_T^i, \hat{v}_T^i), \tag{3.23}$$

$$s_h^i(\hat{u}_h^i, \hat{v}_h^i) := \sum_{T \in \mathcal{T}_h} \big(h_T^{-1}(S_T^i(\hat{u}_T^i), S_T^i(\hat{v}_T^i))_{\partial T^i} + h_T^{-1}(u_T^{k+1}, v_T^{k+1})_{\partial T^D}\big), \tag{3.24}$$

$$\ell_h^i(\hat{v}_h^i) := \sum_{T \in \mathcal{T}_h} (f, v_T^{k+1})_T + (g_N, v_T^{k+1})_{\partial T^N} - (g_D, \boldsymbol{n}_T \cdot \nabla R_T^i(\hat{v}_T^i) - h_T^{-1} v_T^{k+1})_{\partial T^D}. \tag{3.25}$$

In the HHO-N method, we need to add the term $(g_D, h_T^{-1} v_T^{k+1})_{L^2(\partial T^D)}$ into ℓ_T^i for obtaining the consistency for Nitsche's method, see chapter 4 for more details.

Finally, the discrete problem can be defined as follows :

$$\begin{cases} \text{Find } \hat{u}_h \in \hat{V}_h^i \text{ such that} \\ a_h^i(\hat{u}_h, \hat{v}_h) = \ell_h^i(\hat{v}_h), \ \forall \hat{v}_h \in \hat{V}_h^i, \end{cases} \tag{3.26}$$

Remark 3.4. *Unlike the the equal-order HHO or the mixed-order HHO, in which face unknowns are attached on the domain boundary, HHO-N method does not contain any face unknowns on the domain boundary. If the domain boundary has a lot of geometric features (e.g. it is formed by 1 million segments), we need to assign face unknowns on those faces and it may significantly affect the computational efficiency, since face unknowns on the*

Neumann boundary has to be computed in the global coupled linear system. Moreover, if the domain boundary is curved, computing the nonlinear mapping for the boundary conditions has to be applied, which is highly non-trivial. However, HHO-N method does not suffer from these difficulties.

Remark 3.5. *There is another choice for HHO-N method which does not contain the lifting technique, see section 2 in [11]. Without using the lifting operator, the method in [11] is not able to achieve the stability unless the penalty parameter is chosen large enough. (Which is not the case in the presented HHO-N method) In addition, that HHO-Nitsche method employs the face unknowns in the Neumann boundary condition, which is not easy to apply for the PDEs on curve domain. This is due to the computation of the nonlinear mapping arising from the curved faces.*

4. Analysis

In this section, we will present the detailed stability analysis and error analysis in both norms for the HHO-N method. As the analysis of the equal-order HHO, mixed-order HHO are similar and simpler than the HHO-N method, we omit the details on the analysis for other two methods. This chapter is organized as follows : First, we prove the equivalence between energy norm and discrete norm, which shows the stability and well-posedness of discrete problem (3.26). Next, we derive the consistency error and error estimate for the HHO solutions in the (Broken) H^1 type norms. Finally, I present a L^2 error estimate for the proposed HHO-N methods for the problem with mixed boundary condition which first time appeared in the HHO literature.

4.1. Stability and well-posedness

For all $T \in \mathcal{T}_h$ and all $\hat{v}_T^i \in \hat{V}_T^i$, we define the local seminorm

$$|\hat{v}_T^i|_{V_T^i}^2 := \|\nabla v_T^{k+1}\|_T^2 + h_T^{-1}\|v_{\partial T^i}^k - v_T^{k+1}\|_{\partial T^i}^2 + h_T^{-1}\|v_T^{k+1}\|_{\partial T^D}^2. \tag{4.1}$$

Lemma 4.1 (stability)**.** *Let Assumption 2.1 be fulfilled. We have*

$$|\hat{v}_T^i|_{V_T^i}^2 \lesssim a_T^i(\hat{v}_T^i, \hat{v}_T^i) \lesssim |\hat{v}_T^i|_{V_T^i}^2. \tag{4.2}$$

proof. Lower bound : Using the definition of R_T^i, Cauchy-Schwarz inequality and discrete trace inequality (Lemma 2.1), noticing $\nabla v_T^{k+1} \cdot \boldsymbol{n}_T \in \mathbb{P}_{k,d}(T)$, we have

$$\begin{aligned}
\|\nabla v_T^{k+1}\|_T^2 &= (\nabla v_T^{k+1}, \nabla v_T^{k+1})_T \\
&= (\nabla R_T^i(v_T^{k+1}), \nabla v_T^{k+1}) - (v_{\partial T^i}^k - v_T^{k+1}, \nabla v_T^{k+1} \cdot \boldsymbol{n}_T)_{\partial T^i} + (v_T^{k+1}, \nabla v_T^{k+1} \cdot \boldsymbol{n}_T)_{\partial T^D} \\
&\leq \big(\|\nabla R_T^i(v_T^{k+1})\|_T + h_T^{-\frac{1}{2}}\|\Pi_{\partial T^i}^k(v_{\partial T^i}^k - v_T^{k+1})\|_{\partial T^i} + h_T^{-\frac{1}{2}}\|v_T^{k+1}\|_{\partial T^D}\big)\|\nabla v_T^{k+1}\|_T,
\end{aligned}$$

we have the lower bound $\|\nabla v_T^{k+1}\|_T \leq a_T^i(\hat{v}_T^i, \hat{v}_T^i)$. Then we only need to estimate $\|v_{\partial T^i}^k - v_T^{k+1}\|_{\partial T^i}$. We have $v_{\partial T^i}^k - v_T^{k+1} = \Pi_{\partial T^i}^k(v_{\partial T^i}^k - v_T^{k+1}) + (I - \Pi_{\partial T^i}^k)(v_T^{k+1})$, recall the definition

of a_T^i, it rests $(I - \Pi_{\partial T^i}^k)(v_T^{k+1})$ to bound. Invoking the discrete trace inequality and the discrete Poincaré inequality (2.7), we have

$$\begin{aligned}
&h_T^{-1}\|(I - \Pi_{\partial T^i}^k)(v_T^{k+1})\|_{\partial T^i}^2 \\
&\leq h_T^{-1}\|(I - \Pi_{\partial T^i}^0)(v_T^{k+1})\|_{\partial T^i}^2 \leq h_T^{-1}\|(I - \Pi_{\partial T^i}^0)(v_T^{k+1} - \Pi_T^0 v_T^{k+1})\|_{\partial T^i}^2 \\
&\leq h_T^{-1}\|v_T^{k+1} - \Pi_T^0 v_T^{k+1}\|_{\partial T^i}^2 \lesssim h_T^{-2}\|v_T^{k+1} - \Pi_T^0 v_T^{k+1}\|_T^2 \lesssim \|\nabla v_T^{k+1}\|_T^2.
\end{aligned}$$

Upper bound : As lower bound, using the definition of R_T^i, the Cauchy-Schwarz inequality and the discrete trace inequality (Lemma 2.1), we have $\|\nabla R_T^i(v_T^{k+1})\|_T \lesssim |\hat{v}_T^i|_{V_T^i}$. For stabilization term, the stability of L^2- projection directly gives us the bound $h_T^{-\frac{1}{2}}\|S_T^i(\hat{v}_T^i)\|_{\partial T} \lesssim |\hat{v}_T^i|_{V_T^i}$. ■

Let's define $\|\hat{v}_h^i\|_{a_h^i}^2 := \sum_{T\in\mathcal{T}_h} |\hat{v}_T^i|_{a_T^i}$. Using the classical argument, it shows $\|\cdot\|_{a_h^i}^2$ is a norm on $\hat{V}_h^i$, see chapter 39 of [24] for details.

Lemma 4.2 (well-posedness)**.** *Let $u \in H^{3/2+\epsilon}$, with $\epsilon > 0$, to be the solution of the problem* (2.1)*. Then, the discrete problem (3.26) is well-posed.*

proof. The coercivity follows by summing over the mesh cells the bound from Lemma 4.1, and the well-posedness follows from the Lax-Milgram lemma. ■

4.2. Consistency and H^1 error estimate

For $T \in \mathcal{T}_h$, we define the local reduction operator $\hat{I}_T^i : H^1(K) \to \mathbb{P}_{k+1,d}(T)$, for all $u \in H^1(T)$,

$$\hat{I}_T^i(v) := (\Pi_T^{k+1}(v), \Pi_{\partial T^i}^k(v)) \in \hat{V}_T^i. \tag{4.3}$$

We then define the energy projection operator $\mathcal{E}_T : H^1(T) \to \mathbb{P}_{k+1,d}(T)$ such that

$$\mathcal{E}_T(v) := R_T^i \circ \hat{I}_T^i(v) + L_T^{k+1}(v), \qquad \forall v \in H^1(T). \tag{4.4}$$

For convenience, the global energy projection is defined as $\mathcal{E}|_T := \mathcal{E}_T$, $\forall T \in \mathcal{T}_h$.

Lemma 4.3 (Energy projection)**.** *Let $\mathcal{E}_T$ to be the energy projection, the following relation*

holds,

$$(\nabla(\mathcal{E}_T(v)-v),\nabla q)_T=(\Pi_T^{k+1}(v)-v,\nabla q\cdot\boldsymbol{n}_T)_{\partial T^N}, \tag{4.5}$$

and $(\mathcal{E}_T(v),1)_T=(v,1)_T$ *for all* $q\in V_T^{k+1}$ *and all* $v\in H^1(T)$.

proof. Let $v\in H^1(T)$ and $\phi:=R_T^i\circ\hat{I}_T^i(v)=(\Pi_T^{k+1}(v),\Pi_{\partial T^i}^k(v))$. Using the definition of the reconstruction operator, we infer that for all $q\in V_T^{k+1}$,

$$\begin{aligned}(\nabla\phi,\nabla q)_T&=-(\Pi_T^{k+1}(v),\Delta q)_T+(\Pi_{\partial T^i}^k(v),\nabla q\cdot\boldsymbol{n}_T)_{\partial T^i}+(\Pi_T^{k+1}(v),\nabla q\cdot\boldsymbol{n}_T)_{\partial T^N}\\&=-(v,\Delta q)_T+(v,\nabla q\cdot\boldsymbol{n}_T)_{\partial T^i}+(v,\nabla q\cdot\boldsymbol{n}_T)_{\partial T^N}+(\Pi_T^{k+1}(v)-v,\nabla q\cdot\boldsymbol{n}_T)_{\partial T^N}\\&=(\nabla v,\nabla q)_T-(v,\nabla q\cdot\boldsymbol{n}_T)_{\partial T^D}+(\Pi_T^{k+1}(v)-v,\nabla q\cdot\boldsymbol{n}_T)_{\partial T^N},\end{aligned}$$

since $\nabla q\cdot\boldsymbol{n}_T$ is a polynomial of order k. Then, using the definition of lifting operator, we have $(v,\nabla q\cdot\boldsymbol{n}_T)_{\partial T^D}=(\nabla L_T^{k+1}(v),\nabla q)_T$, this gives $(\nabla(\mathcal{E}_T(v)-v),\nabla q)_T=(\Pi_T^{k+1}(v)-v,\nabla q\cdot\boldsymbol{n}_T)_{\partial T^N}$.

Moreover, $(R_T^i\circ\hat{I}_T^i(v)+L_T^{k+1}(g_D),1)_T=(\Pi_T^{k+1}(v),1)_T=(v,1)_T$ by the definition of the reconstruction operator. ■

Remark 4.1. *This property also holds true if our cell unknowns use the same degree as face unknowns. But in that case, the optimal convergence property can not hold since* $(\Pi_T^k(v)-v,\nabla q\cdot\boldsymbol{n}_T)_{\partial T^N}$ *has one order less in approximation of convergence rate comparing with* $(\Pi_T^{k+1}(v)-v,\nabla q\cdot\boldsymbol{n}_T)_{\partial T^N}$.

Remark 4.2. *The term* $(\Pi_T^{k+1}(v)-v,\nabla q\cdot\boldsymbol{n}_T)_{\partial T^N}$ *comes from the Neumann boundary, if problem is defined with a pure Dirichlet boundary condition, this term will disappear. So this property is different from the projection used in the HHO-N method in [11], which has the inconsistency error defined on Dirichlet boundary.*

We start with the approximation property of reconstruction operator.

Lemma 4.4 (approximation for the gradient of reconstruction)**.** *For all* $v\in H^{t+1}(\Omega), t>\frac{1}{2}$ *and* $v|_T\in H^{k+2}(T)$ *for all* $T\in\mathcal{T}_h$, *we have*

$$\|\nabla(\mathcal{E}_T(v)-v)\|_T+h_T^{\frac{1}{2}}\|\nabla(\mathcal{E}_T(v)-v)\|_{\partial T^i\cup\partial T^D}\lesssim h_T^{k+1}|v|_{H^{k+2}(T)}. \tag{4.6}$$

proof. Let us split $\mathcal{E}_T(v)-v := \mathcal{E}_T(v)-\Pi_T^{k+1}(v)+\Pi_T^{k+1}(v)-v$. Using the energy projection (4.5), discrete trace inverse inequality (2.5), approximation properties (2.7) and Cauchy-Schwarz inequality, we have

$$
\begin{aligned}
&\|\nabla(\mathcal{E}_T(v)-\Pi_T^{k+1}(v))\|_T^2\\
&=(\nabla(\mathcal{E}_T(v)-v),\nabla(\mathcal{E}_T(v)-\Pi_T^{k+1}(v)))_T+(\nabla(v-\Pi_T^{k+1}(v))),\nabla(\mathcal{E}_T(v)-\Pi_T^{k+1}(v)))_T\\
&=(\Pi_T^{k+1}(v)-v,\boldsymbol{n}_T\cdot\nabla(\mathcal{E}_T(v)-\Pi_T^{k+1}(v)))_{\partial T^N}+(\nabla(v-\Pi_T^{k+1}(v))),\nabla(\mathcal{E}_T(v)-\Pi_T^{k+1}(v)))_T\\
&\le\Big(h^{-\frac{1}{2}}\|\Pi_T^{k+1}(v)-v\|_{\partial T^N}+\|\nabla(v-\Pi_T^{k+1}(v))\|_T\Big)\|\nabla(\mathcal{E}_T(v)-\Pi_T^{k+1}(v))\|_T\\
&\lesssim h_T^t|v|_{H^{t+1}(T)}\times\|\nabla(\mathcal{E}_T(v)-\Pi_T^{k+1}(v))\|_T,
\end{aligned}
$$

Using the triangle inequality and the approximation properties then proves this lemma.

■

Lemma 4.5 (approximation for the stabilization operator)**.** *For all $v\in H^{t+1}(\Omega), t>\frac{1}{2}$, we have*

$$
h_T^{-\frac{1}{2}}\|S_T^i(\hat{I}_T^i(v))\|_{\partial T^i}+h_T^{-\frac{1}{2}}\|S_T^D(\hat{I}_T^i(v))-v|_{T^D}\|_{\partial T^D}\lesssim\|\nabla(v-\Pi_T^{k+1}(v))\|_T. \tag{4.7}
$$

proof. On the interior faces, using the multiplicative trace inequality (2.6) and approximation properties(2.7), we have

$$
\begin{aligned}
h_T^{-\frac{1}{2}}\|S_T^i(\hat{I}_T^i(v))\|_{\partial T^i}&=h_T^{-\frac{1}{2}}\|\Pi_{\partial T^i}^k(\Pi_T^{k+1}(v)-v)\|_{\partial T^i}\\
&\le h_T^{-\frac{1}{2}}\|\Pi_T^{k+1}(v)-v\|_{\partial T^i}\lesssim\|\nabla(v-\Pi_T^{k+1}(v))\|_T.
\end{aligned}
$$

similarly, on the Dirichlet faces, we have

$$
h_T^{-\frac{1}{2}}\|S_T^D(\hat{I}_T^i(v))-v|_{\partial T^D}\|_{\partial T^D}=h_T^{-\frac{1}{2}}\|\Pi_T^{k+1}(v)-v\|_{\partial T^D}\lesssim\|\nabla(v-\Pi_T^{k+1}(v))\|_T.
$$

■

Lemma 4.6 (consistency and boundedness)**.** *For all $\hat{v}_h^i\in\hat{V}_h^i$, we define the consistency error as $\mathcal{D}_h(\hat{v}_h^i):=\sum_{T\in\mathcal{T}_h}\left(a_T^i(\hat{I}_T^i(u),\hat{v}_T^i)-\ell_T^i(\hat{v}_T^i)\right)$. Assume that $u\in H^{t+1}(\Omega)$ with $t>\frac{1}{2}$*

and $v|_T \in H^{k+2}(T)$ *for all* $T \in \mathcal{T}_h$. *Then we have*

$$|\mathcal{D}_h(\hat{v}_h^i)| \leq (\sum_{T\in\mathcal{T}_h} \|g_T\|_{*T}^2 + \|\xi_T\|_{\#T}^2)^{\frac{1}{2}} \times \|\hat{v}_h^i\|_{a_h^i},$$

where

$$\|g_T\|_{*T}^2 := \|\nabla(v - \mathcal{E}(v))\|_T^2 + h_T\|\nabla(v - \mathcal{E}(v))\|_{\partial T^i \cup \partial T^D}^2, \tag{4.8}$$

$$\|\xi_T\|_{\#T}^2 := h_T^{-1}\|u - \Pi_T^{k+1}(u)\|_{\partial T^i}^2 + h_T^{-1}\|u - \Pi_T^{k+1}(u)\|_{\partial T^D}^2. \tag{4.9}$$

proof. Rearranging the terms, using PDE satisfied by the exact solution and the definition of lifting operator, we have $\mathcal{D}_h(\hat{v}_h^i) = \Psi_1 + \Psi_2$ with

$$\begin{aligned}\Psi_1 := \sum_{T\in\mathcal{T}_h} \big((\nabla R_T^i \circ \hat{I}_T^i(u), \nabla R_T^i(\hat{v}_h^i))_T + (\Delta u, v_T^{k+1})_T \\ + (\nabla L_T^{k+1}(g_D), \nabla R_T^i(\hat{v}_h^i))_T - (g_N, v_T^{k+1})_{\partial T^N}\big),\end{aligned} \tag{4.10}$$

$$\Psi_2 := \sum_{T\in\mathcal{T}_h} \big(h_T^{-1}(S_T^i \circ \hat{I}_T^i(u), S_T^i(\hat{v}_h^i))_{\partial T^i} + h_T^{-1}(\Pi_T^{k+1}(u) - g_D, v_T^{k+1})_{\partial T^D}\big). \tag{4.11}$$

Using the exact solution of PDE, $\sum_{T\in\mathcal{T}_h}(\nabla u \cdot \boldsymbol{n}_T, v_{\partial T^i}^k)_{\partial T^i} = 0$, and the definition of the reconstruction operator, we have

$$\begin{aligned}\Psi_1 = \sum_{T\in\mathcal{T}_h} \big(- (\nabla(\mathcal{E}(u) - u) \cdot \boldsymbol{n}_T, v_T^{k+1})_{\partial T^D} \\ + (\nabla(\mathcal{E}(u) - u), \nabla v_T^{k+1})_T + (\nabla(\mathcal{E}(u) - u) \cdot \boldsymbol{n}_T, v_{\partial T^i}^k - v_T^{k+1})_{\partial T^i}\big)\end{aligned}$$

Noticing $u = g_D$ on Γ_D, we have

$$\Psi_2 = \sum_{T\in\mathcal{T}_h} \big(h_T^{-1}(\Pi_{\partial T^i}^k(u - \Pi_T^{k+1}(u)), v_{\partial T^i}^k - v_T^{k+1})_{\partial T^i} + h_T^{-1}(\Pi_T^{k+1}(u) - u, v_T^{k+1})_{\partial T^D}\big)$$

Then, the Cauchy-Schwarz inequality and discrete trace inverse inequality (2.5) finish this proof. ■

Lemma 4.7 (Broken H^1 error estimate for u_T^{k+1})**.** *For all* $v \in H^{t+1}(\Omega), t > \frac{1}{2}$ *and* $v|_T \in$

$H^{k+2}(T)$ *for all* $T \in \mathcal{T}_h$*, we have*

$$\sum_{T\in\mathcal{T}_h} \|\nabla(u - u_T^{k+1})\|_T^2 \lesssim \Big(\sum_{T\in\mathcal{T}_h} h_T^{2(k+1)} |u|^2_{H^{k+2}(T)}\Big). \tag{4.12}$$

proof. For all $T \in \mathcal{T}_h$, we define the discrete error $\hat{e}_h \in \hat{V}_h^i$ such that $\hat{e}_h := (e_{\mathcal{T}_h}, e_{\mathcal{F}_h^i}) := \hat{I}_h^i(u) - \hat{u}_h^i \in \hat{V}_h^i$. Then using the definition of $\mathcal{D}_h$, we have $\mathcal{D}_h(\hat{e}_h) = a_h^i(\hat{e}_h, \hat{e}_h)$. Using the coercivity in Lemma 4.1 and the consistency in Lemma 4.6 of a_h^i shows

$$\|\hat{e}_h\|^2_{a_h^i} \lesssim a_h^i(\hat{e}_h, \hat{e}_h) = \mathcal{D}_h(\hat{e}_h) \lesssim \sum_{T\in\mathcal{T}_h} \big(\|g_T\|^2_{*T} + \|\xi_T\|^2_{\#T}\big) \times \|\hat{e}_h\|_{a_h^i}.$$

Since $\nabla(u - u_T^{k+1}) = \nabla(u - \Pi_T^{k+1}(u)) + \nabla e_T$, invoking the triangle inequality leads to $\sum_{T\in\mathcal{T}_h} \|\nabla(u - u_T^{k+1})\|_T^2 \lesssim \sum_{T\in\mathcal{T}_h} \big(\|\nabla(u - \Pi_T^{k+1}(u))\|_T^2 + (\|g_T\|^2_{*T} + \|\xi_T\|^2_{\#T})\big)$. Then, the approximation results in (2.7), the we derived the result.

■

Lemma 4.8 (discrete H^1 error estimate)**.** *For all* $v \in H^{t+1}(\Omega), t > \frac{1}{2}$ *and* $v|_T \in H^{k+2}(T)$ *for all* $T \in \mathcal{T}_h$*, let* $\hat{u}_h^i \in \hat{V}_h^i$ *be the HHO solution. Then, we have*

$$\|\hat{e}_h\|_{a_h^i} \lesssim \|\nabla R_h^i(\hat{e}_h)\|_\Omega + s_h^i(\hat{e}_h, \hat{e}_h)^{\frac{1}{2}} \lesssim \Big(\sum_{T\in\mathcal{T}_h} \|g_T\|^2_{*T} + \|\xi_T\|^2_{\#T}\Big)^{\frac{1}{2}} \lesssim \Big(\sum_{T\in\mathcal{T}_h} h_T^{2(k+1)} |u|^2_{H^{k+2}(T)}\Big)^{\frac{1}{2}}. \tag{4.13}$$

proof. We have $a_h^i(\hat{e}_h, \hat{e}_h) = \mathcal{D}_h(\hat{e}_h)$. The stability (Lemma 4.1), approximation properties (lemma 2.3), stability (Lemma 4.1) and Lemma 4.4 infer

$$\begin{aligned}\|\hat{e}_h\|^2_{a_h^i} \lesssim a_h^i(\hat{e}_h, \hat{e}_h) = \mathcal{D}_h(\hat{e}_h) &\lesssim \Big(\sum_{T\in\mathcal{T}_h} \|g_T\|^2_{*T} + \|\xi_T\|^2_{\#T}\Big)^{\frac{1}{2}} \times \|\hat{e}_h\|_{a_h^i} \\ &\lesssim \Big(\sum_{T\in\mathcal{T}_h} h_T^{2(k+1)} |u|^2_{H^{k+2}(T)}\Big)^{\frac{1}{2}} \times \|\hat{e}_h\|_{a_h^i}.\end{aligned}$$

■

Theorem 4.1 (H^1 error estimate for the reconstruction operator)**.** *For all* $v \in H^{t+1}(\Omega), t >$

$\frac{1}{2}$ *and* $v|_T \in H^{k+2}(T)$ *for all* $T \in \mathcal{T}_h$*, we have*

$$\sum_{T\in\mathcal{T}_h} \|\nabla(u - R_T^i(\hat{u}_h^i) - L_T^{k+1}(g_D))\|_T^2 \lesssim \Big(\sum_{T\in\mathcal{T}_h} h_T^{2(k+1)} |u|^2_{H^{k+2}(T)}\Big). \tag{4.14}$$

proof. Noticing that $u - R_T^i(\hat{u}_h^i) - L_T^{k+1}(g_D) = u - R_T^i \circ \hat{I}_T^i(u) - L_T^{k+1}(g_D) + R_T^i \circ \hat{I}_T^i(u) - R_T^i(\hat{u}_h^i)$, using Lemmas 4.6 and 4.1 show

$$\begin{aligned}
&\sum_{T\in\mathcal{T}_h} \|\nabla(u - R_T^i(\hat{u}_h^i) - L_T^{k+1}(g_D))\|_T^2 \\
&\lesssim \sum_{T\in\mathcal{T}_h} \Big(\|\nabla(u - R_T^i \circ \hat{I}_T^i(u) - L_T^{k+1}(g_D))\|_T^2 + \|\nabla(R_T^i \circ \hat{I}_T^i(u) - R_T^i(\hat{u}_h^i))\|_T^2\Big) \\
&\lesssim \sum_{T\in\mathcal{T}_h} \Big(\|g_T\|_{*T}^2 + \|\xi_T\|_{\#T}^2\Big).
\end{aligned}$$

Finally, we derived the final error bound by the approximation results in (2.7). ■

4.3. L^2 error estimate

In order to derive L^2 error estimate, we need to introduce the following dual problem

$$-\Delta\zeta_e = e_{\mathcal{T}_h} \qquad \text{in} \quad \Omega, \tag{4.15}$$

$$\zeta_e = 0 \qquad \text{on} \quad \Gamma_D, \tag{4.16}$$

$$\nabla\zeta_e \cdot \boldsymbol{n} = 0 \qquad \text{on} \quad \Gamma_N. \tag{4.17}$$

Assuming the domain is convex and the elliptic regularity property holds, such that $\|\zeta_e\|_{H^2(\Omega)} \lesssim \|e_{\mathcal{T}_h}\|_\Omega$, see [25] for detail.

Theorem 4.2 (discrete L^2 error estimate)**.** *Let* u *be the exact solution and* $\hat{u}_h^i$ *be the HHO solution. Let* $v \in H^{k+2}(\Omega)$*,* $k \geq 0$ *and the above elliptic regularity property. Using the PDE satisfied by the dual problem, we have*

$$\|e_{\mathcal{T}_h}\|_\Omega \lesssim h^{k+2} |u|_{H^{k+2}(\Omega)}. \tag{4.18}$$

proof. Let ζ_e be the solution of the dual problem (4.15). We have

$$\|e_{\mathcal{T}_h}\|_\Omega^2 = \sum_{T\in\mathcal{T}_h}(e_T, -\Delta\zeta_e)_T = \sum_{T\in\mathcal{T}_h}\big((\nabla e_T, \nabla\zeta_e)_T + (e_{\partial T^i} - e_T, \nabla\zeta_e\cdot\boldsymbol{n}_T)_{\partial T^i} + (-e_T, \nabla\zeta_e\cdot\boldsymbol{n}_T)_{\partial T^D}\big).$$

Let $\zeta = \zeta_e - \mathcal{E}(\zeta_e)$, the energy projection (4.4) shows $(\nabla\mathcal{E}(\zeta_e) - \zeta_e), \nabla e_T)_T = (\Pi_T^{k+1}(\zeta_e) - \zeta_e, \nabla e_T\cdot\boldsymbol{n}_T)_{\partial T^N}$. Then, using the definition of the reconstruction operator, we have

$$\begin{aligned}
\|e_{\mathcal{T}_h}\|_\Omega^2 &= \sum_{T\in\mathcal{T}_h}\big((\nabla e_T, \nabla\zeta_e)_T + (e_{\partial T^i} - e_T, \nabla\zeta_e\cdot\boldsymbol{n}_T)_{\partial T^i} + (-e_T, \nabla\zeta_e\cdot\boldsymbol{n}_T)_{\partial T^D}\big)\\
&= \sum_{T\in\mathcal{T}_h}\big((\nabla e_T, \nabla\zeta)_T + (\nabla e_T, \nabla R_T^i\circ\hat{I}_h^i(\zeta_e))_T + (e_{\partial T^i} - e_T, \nabla\zeta_e\cdot\boldsymbol{n}_T)_{\partial T^i} + (-e_T, \nabla\zeta_e\cdot\boldsymbol{n}_T)_{\partial T^D}\big)\\
&= \sum_{T\in\mathcal{T}_h}\big((\nabla e_T, \nabla\zeta)_T + (\nabla R_T^i(\hat{e}_T), \nabla R_T^i\circ\hat{I}_h^i(\zeta_e))_T + (e_{\partial T^i} - e_T, \nabla\zeta\cdot\boldsymbol{n}_T)_{\partial T^i}\\
&\quad - (e_T, \nabla\zeta\cdot\boldsymbol{n}_T)_{\partial T^D}\big) = \mathcal{I}_1 + \mathcal{I}_2,
\end{aligned}$$

where we used $\zeta = \zeta_e - \mathcal{E}(\zeta_e)$ and the definition of the reconstruction operator for $\hat{e}_T$ in the third line, with

$$\begin{aligned}
\mathcal{I}_1 &:= \sum_{T\in\mathcal{T}_h}\big((\nabla e_T, \nabla\zeta)_T + (e_{\partial T^i} - e_T, \nabla\zeta\cdot\boldsymbol{n}_T)_{\partial T^i} + (-e_T, \nabla\zeta\cdot\boldsymbol{n}_T)_{\partial T^D}\big),\\
\mathcal{I}_2 &:= \sum_{T\in\mathcal{T}_h}(\nabla R_T^i(\hat{e}_T), \nabla R_T^i\circ\hat{I}_h^i(\zeta_e))_T.
\end{aligned}$$

We firstly derive the bound for $\mathcal{I}_1$. Using the Cauchy-schwarz inequality gives

$$\begin{aligned}
\mathcal{I}_1 \lesssim \sum_{T\in\mathcal{T}_h}\big(&\|\nabla(\Pi_T^{k+1}(u) - u_T)\|_T\cdot\|\nabla\zeta\|_T\\
&+ h_T^{-\frac{1}{2}}\|e_{\partial T^i} - e_T\|_{\partial T^i}\cdot h_T^{\frac{1}{2}}\|\nabla\zeta\cdot\boldsymbol{n}_T\|_{\partial T^i} + h_T^{-\frac{1}{2}}\|e_T\|_{\partial T^D}\cdot h_T^{\frac{1}{2}}\|\nabla\zeta\cdot\boldsymbol{n}_T\|_{\partial T^D}\big)
\end{aligned}$$

Then, noticing that $\Pi_T^{k+1}(u) - u_T = (\Pi_T^{k+1}(u) - u) + (u - u_T)$ and the elliptic regularity for dual problem which provides one more order for h (i.e., $\|\nabla\zeta\|_\Omega \le h|\zeta_e|_{H^2(\Omega)} \lesssim h\|e_{\mathcal{T}_h}\|_\Omega$), Lemma 2.3, Lemma 4.8 and Lemma 4.7 give $\mathcal{I}_1 \lesssim h^{t+1}|u|_{H^{t+1}(\Omega)}\|e_{\mathcal{T}_h}\|_\Omega$.

Let us now turn to estimate $\mathcal{I}_2$. Using the definition of bilinear form a_h^i, the definition of

$\hat{e}_h$ and the HHO solution $\hat{u}_h$, we have

$$\mathcal{I}_2 = -s_h^i(\hat{e}_h, \hat{I}_h(\zeta_e)) + a_h^i(\hat{e}_h, \hat{I}_h(\zeta_e)) = -s_h^i(\hat{e}_h, \hat{I}_h(\zeta_e)) + \ell_h^i(\hat{I}_h(\zeta_e)) - a_h^i(\hat{I}_h(u), \hat{I}_h(\zeta_e)).$$

Then, invoking the weak form of the problem $(f, \zeta_e)_\Omega = (\nabla u, \nabla\zeta_e)_\Omega - (g_N, \zeta_e)_{\Gamma_N}$ and $(\nabla u, \nabla\zeta_e)_T = (\nabla u, \nabla(\zeta_e - \Pi_T^{k+1}(\zeta_e)))_T + (\nabla u, \nabla\Pi_T^{k+1}(\zeta_e))_T$, we have

$$\begin{aligned}\mathcal{I}_2 =& - s_h^i(\hat{e}_h, \hat{I}_h(\zeta_e)) + \sum_{T\in\mathcal{T}_h} \big((f, \Pi_T^{k+1}(\zeta_e) - \zeta_e)_T + (g_N, \Pi_T^{k+1}(\zeta_e) - \zeta_e)_{\partial T^N} \\ &+ (h_T^{-1}\Pi_T^{k+1}(\zeta_e) - \nabla R_T^i \circ \hat{I}_h^i(\zeta_e)\cdot\boldsymbol{n}_T, g_D)_{\partial T^D} + (\nabla u, \nabla(\zeta_e - \Pi_T^{k+1}(\zeta_e)))_T \\ &+ (\nabla u, \nabla\Pi_T^{k+1}(\zeta_e))_T\big) - a_h^i(\hat{I}_h(u), \hat{I}_h(\zeta_e)).\end{aligned}$$

Since u solves our model problem, $(\nabla u, \nabla(\zeta_e - \Pi_T^{k+1}(\zeta_e)))_T = (-\Delta u, \zeta_e - \Pi_T^{k+1}(\zeta_e))_T + (\nabla u\cdot\boldsymbol{n}_T, \zeta_e - \Pi_T^{k+1}(\zeta_e))_{\partial T} = (f, \nabla(\zeta_e - \Pi_T^{k+1}(\zeta_e)))_T + (\nabla u\cdot\boldsymbol{n}_T, \zeta_e - \Pi_T^{k+1}(\zeta_e))_{\partial T^i\cup\partial T^D} + (g_N, \zeta_e - \Pi_T^{k+1}(\zeta_e))_{\partial T^N}$. Next, we use the definition of the reconstruction operator R_T^i for $R_T^i\circ\hat{I}_h^i(\zeta_e)$ in $a_h^i(\hat{I}_h(u), \hat{I}_h(\zeta_e))$, adding and subtracting $\sum_{T\in\mathcal{T}_h}(\nabla L_T^{k+1}(g_D), \nabla R_T^i\circ\hat{I}_h^i(\zeta_e))_T$ in $\mathcal{I}_2$, using once the definition of the reconstruction operator R_T^i for $-\sum_{T\in\mathcal{T}_h}(\nabla L_T^{k+1}(g_D), \nabla R_T^i \circ \hat{I}_h^i(\zeta_e))_T$ and finally noticing the fact that for any polynomial q of order k, $(q, \Pi_{\partial T^i}^k\zeta_e)_{\partial T^i} = (q, \zeta_e)_{\partial T^i}$, we have

$$\mathcal{I}_2 = \mathcal{I}_3 + \mathcal{I}_4 + \mathcal{I}_5 + \mathcal{I}_6,$$

with

$$\begin{aligned}\mathcal{I}_3 &:= -s_h^i(\hat{e}_h, \hat{I}_h(\zeta_e)),\\ \mathcal{I}_4 &:= \sum_{T\in\mathcal{T}_h}\big((h_T^{-1}\Pi_T^{k+1}(\zeta_e), g_D)_{\partial T^D} - s_h^i(\hat{I}_h(u), \hat{I}_h(\zeta_e))\big),\\ \mathcal{I}_5 &:= \sum_{T\in\mathcal{T}_h}\big((\nabla u\cdot\boldsymbol{n}_T, \zeta_e - \Pi_T^{k+1}(\zeta_e))_{\partial T} - (\nabla(R_T^i\circ\hat{I}_T^i(u) + L_T^{k+1}(g_D))\cdot\boldsymbol{n}_T, \zeta_e - \Pi_T^{k+1}(\zeta_e))_{\partial T^i}\\ &+ (\nabla(R_T^i\circ\hat{I}_T^i(u) + L_T^{k+1}(g_D))\cdot\boldsymbol{n}_T, \Pi_T^{k+1}(\zeta_e))_{\partial T^D}\big),\\ \mathcal{I}_6 &=: \sum_{T\in\mathcal{T}_h}(\nabla(u - R_T^i\circ\hat{I}_T^i(u) - L_T^{k+1}(g_D)), \nabla\Pi_T^{k+1}(\zeta_e))_T.\end{aligned}$$

Using Lemma 4.8, Lemma 4.5 and the elliptic regularity property of the dual problem, $\mathcal{I}_3$

and $\mathcal{I}_4$ can be bounded as

$$\mathcal{I}_3 \lesssim \|\hat{e}_h\|_{a_h^i} \times \sum_{T\in\mathcal{T}_h} \|\nabla(\zeta_e - \Pi_T^{k+1}(\zeta_e))\|_T \lesssim h^{k+1}|u|_{H^{k+2}(\Omega)} \times h\|e_{\mathcal{T}_h}\|_\Omega,$$

$$\begin{aligned}\mathcal{I}_4 &= \sum_{T\in\mathcal{T}_h} \big(- h_T^{-1}(S_T^i \circ \hat{I}_T^i(u), S_T^i \circ \hat{I}_T^i(\zeta_e))_{\partial T^i} - h_T^{-1}(S_D^i \circ \hat{I}_T^i(u) - g_D, S_D^i \circ \hat{I}_T^i(\zeta_e))_{\partial T^D}\big) \\ &\lesssim h^{k+1}|u|_{H^{k+2}(\Omega)} \times h\|e_{\mathcal{T}_h}\|_\Omega.\end{aligned}$$

Noticing that $\zeta_e = 0$ on Γ_D, $\mathcal{I}_5 = \sum_{T\in\mathcal{T}_h}(\nabla(u - R_T^i \circ \hat{I}_T^i(u) - L_T^{k+1}(g_D)) \cdot \boldsymbol{n}_T, \zeta_e - \Pi_T^{k+1}(\zeta_e))_{\partial T^D\cup\partial T^i}$. Then, using the Cauchy-Schwarz inequality, the elliptic regularity property of the dual problem, the discrete trace inequality (Lemma 2.1), Lemma 4.4 and $u - \mathcal{E}(u) = u - \Pi_T^{k+1}(u) + \Pi_T^{k+1}(u) - \mathcal{E}(u)$, we have

$$\mathcal{I}_5 \lesssim (\sum_{T\in\mathcal{T}_h} h_T^{\frac{1}{2}}\|\nabla(u-\mathcal{E}(u))\|_{\partial T^D\cup\partial T^i}) \times h_T^{-\frac{1}{2}}\|\zeta_e - \Pi_T^{k+1}(\zeta_e)\|_{\partial T^D\cup\partial T^i} \lesssim h^{k+1}|u|_{H^{k+2}(\Omega)} \times h\|e_{\mathcal{T}_h}\|_\Omega.$$

Finally, invoke $\nabla\zeta_e \cdot \boldsymbol{n} = 0$ on Γ_N into $\mathcal{I}_6$ and use the energy projection property for ζ_e shows $\mathcal{I}_6 = \sum_{T\in\mathcal{T}_h}(\Pi_T^{k+1}(u) - u, \nabla(\Pi_T^{k+1}(\zeta_e) - \zeta_e) \cdot \boldsymbol{n})_{\partial T^N}$, then, as in $\mathcal{I}_5$, the Cauchy-Schwarz inequality and the discrete trace inequality (2.5) give

$$\mathcal{I}_6 \lesssim (\sum_{T\in\mathcal{T}_h} h_T^{\frac{1}{2}}\|\Pi_T^{k+1}(u) - u\|_{\partial T^N}) \times h_T^{-\frac{1}{2}}\|\nabla(\Pi_T^{k+1}(\zeta_e) - \zeta_e)\|_{\partial T^N} \lesssim h^{k+2}|u|_{H^{k+2}(\Omega)} \times \|e_{\mathcal{T}_h}\|_\Omega,$$

which finishes this proof.

■

Theorem 4.3 (L^2 error estimate for the reconstruction operator)**.** *In the framework of Theorem 4.2, we have*

$$\sum_{T\in\mathcal{T}_h} \|u - R_T^i(\hat{u}_h^i) - L_T^{k+1}(g_D)\|_T \lesssim h^{k+2}|u|_{H^{k+2}(\Omega)}.$$

proof. The triangle inequality and the Poincaré inequality (2.8) give

$$\begin{aligned}
&\sum_{T\in\mathcal{T}_h} \|u - R_T^i(\hat{u}_h^i) - L_T^{k+1}(g_D)\|_T \\
&\leq \sum_{T\in\mathcal{T}_h} \big(\|u - R_T^i \circ \hat{I}_h^i(u) - L_T^{k+1}(g_D)\|_T + \|R_T^i \circ \hat{I}_h^i(u) - R_T^i(\hat{u}_h^i)\|_T\big) \\
&\lesssim \sum_{T\in\mathcal{T}_h} \big(h\|\nabla(u - R_T^i \circ \hat{I}_h^i(u) - L_T^{k+1}(g_D))\|_T + \|R_T^i \circ \hat{I}_h^i(u) - R_T^i(\hat{u}_h^i)\|_T\big).
\end{aligned}$$

The Poincaré inequality also gives $\|v\|_T \lesssim h_T\|\nabla v\|_T + \|\Pi_T^0 v\|_T$ for all $v \in H^1(T)$. Applying this bound to $v := R_h^i \circ \hat{I}_h^i(u) - R_h^i(\hat{u}_h^i)$, and noticing $\Pi_T^0 v = \Pi_T^0\big((R_h^i \circ \hat{I}_h^i(u) + L_T^{k+1}(g_D)) - (R_h^i(\hat{u}_h^i) + L_T^{k+1}(g_D))\big) = \Pi_T^0(u - u_T^{k+1})$, we infer that

$$\sum_{T\in\mathcal{T}_h} \|R_T^i \circ \hat{I}_h^i(u) - R_T^i(\hat{u}_h^i)\|_T \lesssim h \sum_{T\in\mathcal{T}_h} \|\nabla(R_T^i \circ \hat{I}_h^i(u) - R_T^i(\hat{u}_h^i))\|_\Omega + \|e_{\mathcal{T}_h}\|_\Omega,$$

since $\|\Pi_T^0(u - u_T^{k+1})\|_T \leq \|\Pi_T^{k+1}(u - u_T^{k+1})\|_T$ and $\Pi_T^{k+1}(u - u_T^{k+1}) = e_T$. Finally, Theorem 4.2 and Lemma 4.8 finish this proof.

■

Remark 4.3 (Equal-Order Case and Mixed-Order Case)**.** *Theoretical analysis of these two cases are similar to HHO-Nitsche method, the only things we need to change are the definition of norm, the reconstruction operator and the stabilization operator. See [14] for some examples.*

5. Implementation aspect

We present the basic ideas of implementation of the HHO methods, and a few subtle points in the computational aspect will be discussed in this section.

5.1. Basic ideas

In the HHO methods, there are two kind of unknowns, i.e., cell unknowns and face unknowns, so we define $U_{\mathcal{T}}, U_{\mathcal{F}}$ and $U = (U_{\mathcal{T}}, U_{\mathcal{F}})$ as global cell unknowns, global face unknowns and global total unknowns, respectively. The implementation can be divided into tree steps : (1) Computing the local reconstruction operator, the local stabilization operator and the local bilinear form in each cell (which contains also face unknowns). (2) Assembling the global linear system and use static condensation to eliminate the cell unknowns. (3) Solving the global coupled linear system.

Firstly, we need to compute the local reconstruction operator and the stabilisation operator in each cell. We assume that in the HHO finite element space, cell basis are $\{\phi_i\}_{i=0}^{k+1}$ and face basis are $\{\psi_i\}_{i=0}^{k}$, cell unknowns and face unknowns are $\{U_T^{loc}\}_{T\in\mathcal{T}_h}$ and $\{U_F^{loc}\}_{F\in\mathcal{F}}$, respectively. Then we can obtain the matrix form of the local reconstruction operator considering the matrix form of the definition of the reconstruction operator (3.16) or (3.17). We take (3.17) as an example here : we choose q be the cell basis functions, and the expression (3.17) is equivalent to the matrix form $Q^t K_T(R_T U^{loc}) = Q^t V_{R,T} U^{loc}$, where Q^t means the transpose of the vector of the coefficients of our test function q, K_T is the local stiffness matrix $(\nabla\phi_i, \nabla\phi_j)_T$ and $V_{R,T}$ presents the right hand side of (3.17). So we can derive the local reconstruction operator $R_T = K_T^{-1} V_{R,T}$. With the same argument, we can get the matrix form of (3.21) as $Q^t M_{S,T}(S_{S,T} U^{loc}) = Q^t V_{S,T} U^{loc}$ and the matrix form of the local stabilization operator $S_{S,T} = M_{S,T}^{-1} V_{S,T}$. After that, the local bilinear form can be formed as $a_T^i(\hat{v}_T^i, \hat{w}_T^i) = W^t(R_T^t K_T R_T + h_T^{-1} S_{S,T}^t M_{S,T} S_{S,T}) V$ where W and V are the vector of the coefficients of $\hat{w}_T^i$ and $\hat{v}_T^i$ respectively.

Secondly, we can assemble each cell bilinear form into global matrix A defined in the global linear system $AU = b$. The vector b is easily obtained by taking each basis

function into (3.25). And we can add boundary conditions into the domain boundary face unknowns by replacing $U_{\mathcal{F}}$ on the the domain boundary by boundary data g_D and g_N. Then, we find that the global linear system $AU = b$ can be expressed as a block matrix

$$\left[\begin{array}{c|c} A_{\mathcal{T}\mathcal{T}} & A_{\mathcal{T}\mathcal{F}} \\ \hline A_{\mathcal{F}\mathcal{T}} & A_{\mathcal{F}\mathcal{F}} \end{array}\right] \left[\begin{array}{c} U_{\mathcal{T}} \\ \hline U_{\mathcal{F}} \end{array}\right] = \left[\begin{array}{c} b_{\mathcal{T}} \\ \hline b_{\mathcal{F}} \end{array}\right].$$

Then, a simple computation shows this block matrix can be decomposed as 2 small linear systems

$$A_{\mathcal{T}\mathcal{T}}U_{\mathcal{T}} = b_{\mathcal{T}} - A_{\mathcal{T}\mathcal{F}}U_{\mathcal{F}}, \tag{5.1}$$

$$(A_{\mathcal{F}\mathcal{F}} - A_{\mathcal{F}\mathcal{T}}A_{\mathcal{T}\mathcal{T}}^{-1}A_{\mathcal{T}\mathcal{F}})U_{\mathcal{F}} = b_{\mathcal{F}} - A_{\mathcal{F}\mathcal{T}}A_{\mathcal{T}\mathcal{T}}^{-1}b_{\mathcal{T}}. \tag{5.2}$$

Then, we can solve (5.2) firstly, and then solve (5.1). This technique is called the static condensation or the Schur decomposition.

The details of the construction of our matrix and a C++ code of equal-order HHO are discussed in [12].

5.2. Some remarks

Remark 5.1 (Laplacien or gradient)**.** *As we mentioned in chapter 3, (3.1), (3.9) and (3.16) numerically perform better than (3.2), (3.10) and (3.17) respectively, though they are equivalent in the mathematical level. One important reason is that we need to compute one more matrix* $(v_T, \nabla q \cdot \boldsymbol{n}_T)_{\partial T}$ *for our reconstruction operator. Even if it does not influence too much our computational efficiency in each local problem, the sum of these small influences can affect significantly the global computation.*

Remark 5.2 (Equal-order or mixed-order)**.** *Even if we can get the same convergence rate, the numerical experiments show that the mixed-order HHO method performs better than equal-order HHO method in terms of the computational time. One essential reason is that, although the additional order in the cell unknowns of the mixed-order case can increase the computational time for the reconstruction operator, the simplified stabilization operator reduces much more computational time.*

Remark 5.3 (Choice of basis)**.** *Theoretically, the choice of basis does not affect the final*

solution, but in practice, the condition number is related to the choice of basis. When the condition number is too large, the numerical stability may be influenced. If we look at our linear systems (5.1) and (5.2), we can find out that $A_{\mathcal{TT}}$ is block-diagonal, so the accuracy of linear systems (5.1) can be assured and computed efficiently by using parallel computation, but the global coupled linear systems (5.2) $A_{\mathcal{FF}} - A_{\mathcal{FT}} A_{\mathcal{TT}}^{-1} A_{\mathcal{TF}}$ has a stencil depends on the number of face-based neighbours per-cell. Furthermore, the condition number of this matrix will influence the numerical stability of the HHO methods.

Remark 5.4 (Quadrature of general area)**.** *In the HHO-N method, one main challenge is to use the accurate numerical quadrature for approximating the integral on the area containing a curved boundary. In my code, I added enough small edges to approximate the curved boundary such that the numerical integral error between the initial area and the polygon area can be smaller than the approximation error of the proposed HHO-N methods, since we assumed that all curved boundaries are Lipschitz continuous.*

6. Numerical examples

In this chapter and chapter 7, the scale related to the stabilisation term is implemented as $\frac{(k+1)(k+d)}{h_T}$ instead of $\frac{1}{h_T}$.

6.1. Compare between the methods

Let the computational domain $\Omega := (0,1)^2, u = \sin(\pi x)\sin(\pi y) + x^5 + y^5$, the mixed boundary condition is imposed such that, when $x \leq 0.5$, we impose the Dirichlet boundary condition, and when $x > 0.5$, the Neumann boundary condition is imposed. The rectangular mesh is used in this example, the convergence rate is tested with polynomial order $k = 0, 1, 2, 3, 4, 5$ and on 16, 64, 256, 1024, 4096 cells. The numerical experiments in Figure 10.4 and 10.5 show the convergence rate is these rates exactly confirm the theoretical results of Theorems 4.1, 4.2 and 4.3 i.e., for L^2 norm, the rate is $k+2$ and for H^1 norm, the rate is $k+1$. As the linear system is solved by the direct solver, the convergence rate may be deteriorated for the high condition number.

6.2. Compare between the computational Time

The exact solution, computational domain, the mixed boundary condition and the mesh is set as the above example, the computational time are tested by the two HHO methods on 16384 cells with polynomial order $k = 0, 1, 2, 3, 4, 5$. The numerical example shows that the computational time of the mixed-order HHO method is shorter than the equal-order HHO methods. In Figure 10.6, we present the computational time, and the difference of computational time between mixed-order and equal-order is presented in Figure 10.7. We observe from the figures that, the computational time for reconstruction increases 'linearly' but the computational time for stabilization decreases 'quadratically'.

6.3. HHO-N method for some curved boundaries

The HHO-N method is applied to two curved boundaries, one of them is a circle with a hole, another one is a waved rectangle with a hole, see Figure 10.1.

For the first domain, the outer circle has center and radius as $(0,0)$ and 1, the inner circle has center and radius as $(0.1,0)$ and 0.2, $u = \exp(\sin x)\exp(\sin y)$, the mixed boun-

dary condition is imposed such that, on both of inner circle and outer circle, we impose the Dirichlet boundary condition when $x \leq 0.5$, and the Neumann boundary condition is imposed when $x > 0.5$. The triangular mesh is used in this example, the The convergence rate is tested with polynomial order $k = 1, 2, 3$ and on 584, 925, 2336, 6272 cells.

For the second domain, we modified the $[0, 1]^2$ domain by adding a sinus oscillation with amplitude 0.05 in the top and bottom of the square, the inner circle has center and radius as $(0.1, 0)$ and 0.2, $u = \exp(\sin x)\exp(\sin y)$, the mixed boundary condition is imposed such that, on both of inner boundary and outer boundary, we impose the Dirichlet boundary condition when $x \leq 0.5$, and the Neumann boundary condition is imposed when $x > 0.5$. The triangular mesh is used in this example, the The convergence rate is tested with polynomial order $k = 1, 2, 3$ and on 1179, 2093, 3086, 8362 cells.

The convergence result is presented in Figure 10.8. The value of function on the curved boundaries is approximated here by replacing the curved boundary by enough small segments such that the intergal error is smaller than the error of HHO-N method. We can also compute the value on the curved boundaries by doing a nonlinear map from a straight line to the curve, but it requires more computational cost, see [4] for details.

6.4. HHO-N method for complex boundary

HHO-N method is applied to a circle with center $(0, 0)$ and radius 1, with 20 line segments in each boundary cell, see Figure 10.2 for example. $u = \exp(\sin x)\exp(\sin y)$, we impose the Dirichlet boundary condition when $x \leq 0.5$, and the Neumann boundary condition is imposed when $x > 0.5$. The triangular mesh is used in this example, the The convergence rate is tested with polynomial order $k = 1, 2, 3$ and on 661, 1045, 2642, 7184 cells.

The convergence result is presented in Figure 10.9. This example confirms one important advantage of Nitsche's method : When there are too many Neumann boundary (the geometry properties of Neumann boundary are too complex), the face unknowns of Neumann boundary will appear in the final linear system, which makes the linear system too large. By contrast, HHO-N method perfectly avoids this problem since it does not include the face unknowns on Neumann boundary.

6.5. Influence of Basis

We tried 2 kind of basis for the face basis. The first one is the Legendre basis, Another one is the quasi-H^1 orthogonal basis, i.e., $\phi_0 = \frac{1+x}{2}, \phi_1 = \frac{1-x}{2}, \phi_i = \int_{-1}^{x} L_{i-1}(s)ds, i > 1$, with L_i the standard Legendre basis in the interval $[-1, 1]$.

The exact solution, computational domain, the mixed boundary condition, the mesh, the polynomial order and cells are set as the first example of section 6.3 (the only thing changed here is the face basis), the convergence result of the first basis is already presented in Figure 10.8, The convergence result of the second basis can be found in Figure 10.10 . Although they have the same performance of convergence in the mathematical level, the condition number of the quasi-H^1 orthogonal basis is only half of the Legendre basis case, which means the quasi-H^1 orthogonal basis has better computational stability, see Tables 10.1 and 10.2 realized in the circle domain with a hole.

7. Singular-perturbed reaction diffusion problem

In this chapter, we consider a singular-perturbed reaction diffusion model, The theoretical analysis and numerical tests are presented in this chapter.

7.1. Model

We assume a diffusion parameter $\varepsilon \geq 0$ the singular-perturbed parameter, and we consider the following problem

$$-\varepsilon\Delta u + u = f \qquad \text{in} \quad \Omega, \tag{7.1}$$

$$\varepsilon u = \varepsilon g_D \qquad \text{on} \quad \Gamma_D. \tag{7.2}$$

It is convenient to consider the following inner product and corresponding norm on $\varepsilon H^1(S) + L^2(S)$ (this is a shortcut notation for $H^1(S)$ if $\varepsilon > 0$ and $L^2(S)$ if $\varepsilon = 0$) :

$$(w, v)_{S,\varepsilon} := \varepsilon(\nabla w, \nabla v)_S + (w, v)_S, \qquad \|v\|^2_{S,\varepsilon} := (v, v)_{S,\varepsilon}. \tag{7.3}$$

Let us consider the Hilbert spaces $V := \varepsilon H^1(\Omega) + L^2(\Omega)$ and $V_0 := \varepsilon H^1_0(\Omega) + L^2(\Omega)$ equipped with the inner product $(w, v)_{\Omega,\varepsilon}$. By assuming the forcing data in (7.1) satisfying the $f \in L^2(\Omega)$ and the boundary data such that $\varepsilon u_g = \varepsilon g_D$ on Γ_D. The weak formulation for (7.1) is derived : Find $u \in u_g + V_0$ such that

$$(u, v)_{\Omega,\varepsilon} = (f, v)_\Omega, \ \forall v \in V_0. \tag{7.4}$$

By using the Lax-Milgram Lemma, the well-posedness of the above problem is proven.

7.2. The HHO-N method

Similar to the Possion problems, we need to compute the local reconstruction operator, and designing the appropriate stabilization term with the correct dependence of the singular perturbed parameter ε, such that the proposed HHO-N methods will be stable and converge optimally with respect to the full range of $\varepsilon \geq 0$. We define the following

mesh-dependent parameter for measuring the dominant operator in the PDE : For all $T \in \mathcal{T}_h$,

$$\sigma_T = \max\left(\varepsilon, h_T^2\right). \tag{7.5}$$

The reconstruction operator can be defined as $R_T^\varepsilon : \hat{V}_T^i \to \mathbb{P}_{k+1,d}(T)$ s.t. for every pair $\hat{v}_T^i = (v_T^{k+1}, v_{\partial T^i}^k) \in \hat{V}_T^i$, the function $R_T^\varepsilon(\hat{v}_T^i)$ is s.t. for all $q \in \mathbb{P}_{k+1,d}(T)$,

$$\begin{aligned}(R_T^\varepsilon(\hat{v}_T^i), q)_{T,\varepsilon} &:= -\varepsilon(v_T^{k+1}, \Delta q)_T + (v_T^{k+1}, q)_T + \varepsilon(v_{\partial T^i}^k, \boldsymbol{n}_T \cdot \nabla q)_{\partial T^i} &(7.6)\\ &= (v_T^{k+1}, q)_{T,\varepsilon} - \varepsilon(v_T^{k+1} - v_{\partial T^i}^k, \boldsymbol{n}_T \cdot \nabla q)_{\partial T^i} - \varepsilon(v_T^{k+1}, \boldsymbol{n}_T \cdot \nabla q)_{\partial T^D}, &(7.7)\end{aligned}$$

and the lifting operator is defined as $L_T^\varepsilon : L^2(\partial T^D) \to \mathbb{P}_{k+1,d}(T)$ for all $T \in \mathcal{T}_h$ such that, for all $g_D \in L^2(\partial T^D)$ and all $q \in \mathbb{P}_{k+1,d}(T)$,

$$(L_T^\varepsilon(g_D), q)_{T,\varepsilon} := (\varepsilon g_D, \nabla q \cdot \boldsymbol{n}_{\Gamma_D})_{\partial T^D}. \tag{7.8}$$

It is clear that $L_T^\varepsilon(g_D) := 0$ for all interior cell.

For the interior face $F \in \mathcal{F}_{\partial T^i}$ and the Dirichlet face $F \in \mathcal{F}_{\partial T^D}$, the stabilization operators (3.20) and (3.21) are used, respectively. Then, the local bilinear form a_T^ε in each cell T is defined as follow :

$$\begin{aligned}a_T^\varepsilon(\hat{u}_T^i, \hat{v}_T^i) :=& (R_T^\varepsilon(\hat{u}_T^i), R_T^\varepsilon(\hat{v}_T^i))_{T,\varepsilon} + \sigma_T h_T^{-1}(S_T^i(\hat{u}_T^i), S_T^i(\hat{v}_T^i))_{\partial T^i} &(7.9)\\ &+ \varepsilon h_T^{-1}(S_T^D(u_T^{k+1}), S_T^D(v_T^{k+1}))_{\partial T^D}. &(7.10)\end{aligned}$$

Next, we can define the global forms a_h^ε, s_h^ε and ℓ_h^i as follows :

$$a_h^\varepsilon(\hat{u}_h^i, \hat{v}_h^i) := \sum_{T \in \mathcal{T}_h} a_T^\varepsilon(\hat{u}_T^i, \hat{v}_T^i), \tag{7.11}$$

$$s_h^\varepsilon(\hat{u}_h^i, \hat{v}_h^i) := \sum_{T \in \mathcal{T}_h} \left(\sigma_T h_T^{-1}(S_T^i(\hat{u}_T^i), S_T^i(\hat{v}_T^i))_{\partial T^i} + \varepsilon h_T^{-1}(u_T^{k+1}, v_T^{k+1})_{\partial T^D}\right), \tag{7.12}$$

$$\ell_h^\varepsilon(\hat{v}_h^i) := \sum_{T \in \mathcal{T}_h} \left((f, v_T^{k+1})_{L^2(T)} - (\varepsilon g_D, \boldsymbol{n}_T \cdot \nabla R_T^i(\hat{v}_T^i) - h_T^{-1} v_T^{k+1})_{\partial T^D}\right). \tag{7.13}$$

Consequently, we can define the discrete problems as follows

$$\begin{cases} \text{Find } \hat{u}_h \in \hat{V}_h^i \text{ such that} \\ a_h^\varepsilon(\hat{u}_h, \hat{v}_h) = \ell_h^\varepsilon(\hat{v}_h),\ \forall \hat{v}_h \in \hat{V}_h^i. \end{cases} \tag{7.14}$$

Remark 7.1 (Nitsche's method)**.** *When ε trends to zero, space V continuously degenerates to $L^2(\Omega)$. If we strongly impose the boundary condition into our finite element method, i.e. we insert $\varepsilon u = \varepsilon g_D$ directly into our finite element method instead of considering the weak form $(\varepsilon g_D, \nabla v \cdot \boldsymbol{n})_{\Gamma_D}$, the discrete solution will have an oscillation near the domain boundary when ε trends to zero, but if we weakly impose the boundary condition by Nitsche's method, this non-physical oscillation will be eliminated, see [27] for details.*

Remark 7.2 (Stabilization)**.** *One important reason for choosing $\sigma_T = \max\left(\varepsilon, h_T^2\right)$ is that, when ε equals zero and if we set simply $\sigma_T = \varepsilon$, the gradient terms will disappear, the face unknowns will disappear. One of our aim is to make the HHO method robust, i.e., when ε equals zero, $A_{\mathcal{F}\mathcal{F}}$ should not be 0, this deduces that σ_T should be something different. Then, we observe that when ε equals zero, our problem degenerates to a L^2 approximation problem which should has the convergence rate $k+2$, which implies our definition of σ_T.*

7.3. Stability analysis and error estimates

As the analysis is similar to the Poisson case, we will modify some technical details in Chapter 4 and present the analysis for problem (7.1) with the boundary condition (7.2).

Before the discuss of the stability, we define the local seminorm for all $T \in \mathcal{T}_h$ and all $\hat{v}_T^i \in \hat{V}_T^i$ by

$$|\hat{v}_T^i|_{a_T^\varepsilon}^2 := \|v_T^{k+1}\|_{T,\varepsilon}^2 + \sigma_T h_T^{-1} \|v_{\partial T^i}^k - v_T^{k+1}\|_{\partial T^i}^2 + \varepsilon h_T^{-1} \|v_T^{k+1}\|_{\partial T^D}^2. \tag{7.15}$$

Lemma 7.1 (stability and well-posedness)**.** *Let Assumption 2.1 to hold. We have*

$$|\hat{v}_T^i|_{a_T^\varepsilon}^2 \lesssim a_T^\varepsilon(\hat{v}_T^i, \hat{v}_T^i) \lesssim |\hat{v}_T^i|_{a_T^\varepsilon}^2. \tag{7.16}$$

Moreover, the well-posedness of the problem (7.14) *holds true.*

proof. We start with the lower bound. Using the definition of the reconstruction operator,

we have

$$\|v_T^{k+1}\|_{T,\varepsilon}^2 \lesssim \|R_T^\varepsilon(\hat{v}_T^i)\|_{T,\varepsilon}^2 + \varepsilon h_T^{-1}\|\Pi_{\partial T^i}^k(v_{\partial T^i}^k - v_T^{k+1})\|_{\partial T^i}^2 + \varepsilon h_T^{-1}\|v_T^{k+1}\|_{\partial T^D}^2 \lesssim a_T^\varepsilon(\hat{v}_T^i, \hat{v}_T^i).$$

Using the triangle inequality, Poincaré inequality (2.8), multiplicative trace inequality (2.6) and the fact $\sigma_T \leq \varepsilon + h_T^2$, we have

$$\begin{aligned}
&\sigma_T h_T^{-1}\|v_{\partial T^i}^k - v_T^{k+1}\|_{\partial T^i}^2 \lesssim \sigma_T h_T^{-1}\|\Pi_{\partial T^i}^k(v_{\partial T^i}^k - v_T^{k+1})\|_{\partial T^i}^2 + \sigma_T h_T^{-1}\|\Pi_{\partial T^i}^k(v_T^{k+1}) - v_T^{k+1}\|_{\partial T^i}^2 \\
&\lesssim \sigma_T h_T^{-1}\|\Pi_{\partial T^i}^k(v_{\partial T^i}^k - v_T^{k+1})\|_{\partial T^i}^2 + \sigma_T h_T^{-1}\|\Pi_T^k(v_T^{k+1}) - v_T^{k+1}\|_{\partial T^i}^2 \\
&\lesssim \sigma_T h_T^{-1}\|\Pi_{\partial T^i}^k(v_{\partial T^i}^k - v_T^{k+1})\|_{\partial T^i}^2 + (\varepsilon\|\nabla v_T^{k+1}\|_T^2 + \|v_T^{k+1}\|_T^2) \lesssim a_T^\varepsilon(\hat{v}_T^i, \hat{v}_T^i).
\end{aligned}$$

The upper bound can be derived by the same argument as in Lemma 4.1.

Moreover, after establishing the stability of the bilinear form a_T^ε, the well-posedness of the global discrete problem 7.14 can be derived with the same argument as in Lemma 4.2.

■

In this chapter, we define the energy projection operator $\mathcal{E}_T : \varepsilon H^1(T) + L^2(T) \to \mathbb{P}_{k+1,d}(T)$ such that

$$\mathcal{E}_T(v) := R_T^\varepsilon \circ \hat{I}_T^i(v) + L_T^\varepsilon(v), \qquad \forall v \in \varepsilon H^1(T) + L^2(T). \tag{7.17}$$

For convenience, the global energy projection is defined as $\mathcal{E}|_T := \mathcal{E}_T$, $\forall T \in \mathcal{T}_h$.

Lemma 7.2 (energy projection)**.** *For all $v \in \varepsilon H^1(T) + L^2(T)$, we have the following relation,*

$$(\mathcal{E}_T(v) - v, q)_{T,\varepsilon} = 0, \quad \forall q \in V_T^{k+1}. \tag{7.18}$$

proof. The same argument as in Lemma 4.3 proves this lemma, only substitute $(\nabla\phi, \nabla q)_T$ by $(\phi, q)_{T,\varepsilon}$ in Lemma 4.3. ■

Lemma 7.3 (approximation for the gradient of reconstruction)**.** *For all $v \in H^{k+2}(T)$,*

with $T \in \mathcal{T}_h$, we have

$$\|\mathcal{E}_T(v) - v\|_{T,\varepsilon} + \varepsilon^{\frac{1}{2}} h_T^{\frac{1}{2}} \|\boldsymbol{n}_T \cdot \nabla(\mathcal{E}_T(v) - v)\|_{\partial T} \lesssim (\varepsilon^{\frac{1}{2}} h_T^{k+1} + h_T^{k+2}) |v|_{H^{k+2}(T)}. \tag{7.19}$$

proof. We first split the $\mathcal{E}(v) - v = (\mathcal{E}(v) - \Pi_T^{k+1}(v)) + (\Pi_T^{k+1}(v) - v)$. Then using the (7.18) and the Cauchy-Schwarz inequality shows

$$\begin{aligned}
\|\mathcal{E}_T(v) - \Pi_T^{k+1}(v)\|_{T,\varepsilon}^2 &= (v - \Pi_T^{k+1}(v), \mathcal{E}_T(v) - \Pi_T^{k+1}(v))_{T,\varepsilon} \\
&\lesssim \|(v - \Pi_T^{k+1}(v))\|_{T,\varepsilon} \|(\mathcal{E}_T(v) - \Pi_T^{k+1}(v))\|_{T,\varepsilon} \\
&\lesssim (\varepsilon^{\frac{1}{2}} h_T^{k+1} + h_T^{k+2}) |v|_{H^{k+2}(T)} \|(\mathcal{E}_T(v) - \Pi_T^{k+1}(v))\|_{T,\varepsilon}.
\end{aligned}$$

Similarly, using the above result and the discrete trace inequality (2.5) ,

$$\begin{aligned}
\varepsilon^{\frac{1}{2}} h_T^{\frac{1}{2}} \|\boldsymbol{n}_T \cdot \nabla(\mathcal{E}_T(v) - \Pi_T^{k+1}(v))\|_{\partial T} &\lesssim \varepsilon^{\frac{1}{2}} \|\nabla(\mathcal{E}_T(v) - \Pi_T^{k+1}(v))\|_T \\
&\lesssim \|(\mathcal{E}_T(v) - \Pi_T^{k+1}(v))\|_{T,\varepsilon} \lesssim (\varepsilon^{\frac{1}{2}} h_T^{k+1} + h_T^{k+2}) |v|_{H^{k+2}(T)}.
\end{aligned}$$

Finally, using the triangle inequality and the approximation results (2.7), the bound (7.3) is derived. ■

Lemma 7.4 (approximation for the stabilization operator)**.** *For each cell $T \in \mathcal{T}_h$ and $v \in \varepsilon H^1(T) + L^2(T)$, we have*

$$\sigma_T^{\frac{1}{2}} h_T^{-\frac{1}{2}} \|S_T^i(\hat{I}_T^i(v))\|_{\partial T^i} \lesssim \|v - \Pi_T^{k+1}(v)\|_{T,\varepsilon}. \tag{7.20}$$

In addition, for the Dirichlet boundary, we also have

$$\varepsilon^{\frac{1}{2}} h_T^{-\frac{1}{2}} \|S_T^D(\Pi_T^{k+1}(v)) - v\|_{\partial T^D} \lesssim \varepsilon^{\frac{1}{2}} \|\nabla(v - \Pi_T^{k+1}(v))\|_T. \tag{7.21}$$

proof. Using the stability of the L^2-projection, Poincaré inequality (2.8), multiplicative

trace inequality (2.6) and the fact $\sigma_T \leq \varepsilon + h_T^2$, we have

$$\begin{aligned}\sigma_T h_T^{-1}\|S_T^i(\hat{I}_T^i(v))\|_{\partial T^i}^2 &= \sigma_T h_T^{-1}\|\Pi_{\partial T^i}^k(\Pi_T^{k+1}(v)-v)\|_{\partial T^i}^2 \\ &\lesssim \varepsilon h_T^{-1}\|\Pi_T^{k+1}(v)-v\|_{\partial T^i}^2 + h_T\|\Pi_T^{k+1}(v)-v\|_{\partial T^i}^2 \\ &\lesssim \varepsilon\|\nabla(\Pi_T^{k+1}(v)-v)\|_T^2 + \|\Pi_T^{k+1}(v)-v\|_T^2 \lesssim \|v-\Pi_T^{k+1}(v)\|_{T,\varepsilon}^2.\end{aligned}$$

The derivation of (7.21) follows the same argument.

■

Lemma 7.5 (consistency and boundedness)**.** *For all $\hat{v}_h^i \in \hat{V}_h^i$, we define the consistency error as $\mathcal{D}_h^\varepsilon(\hat{v}_h^i) := \sum_{T\in\mathcal{T}_h}\big(a_T^\varepsilon(\hat{I}_T^i(u),\hat{v}_T^i) - \ell_T^\varepsilon(\hat{v}_T^i)\big)$. Assume that $u \in H^{1+t}(\Omega)$ with $t > \frac{1}{2}$. Then we have*

$$|\mathcal{D}_h^\varepsilon(\hat{v}_h^i)| \leq \Big(\sum_{T\in\mathcal{T}_h}\|g_T^\varepsilon\|_{*T}^2 + \|\xi_T^\varepsilon\|_{\#T}^2\Big)^{\frac{1}{2}} \times \|\hat{v}_h^i\|_{a_h^\varepsilon},$$

where

$$\|g_T^\varepsilon\|_{*T}^2 := \|v-\mathcal{E}_T(v)\|_{T,\varepsilon}^2 + \varepsilon h_T\|\boldsymbol{n}_T\cdot\nabla(v-\mathcal{E}_T(v))\|_{\partial T}^2, \tag{7.22}$$

$$\|\xi_T^\varepsilon\|_{\#T}^2 := \sigma_T h_T\|u-\Pi_T^{k+1}(u)\|_{\partial T^i}^2 + \varepsilon h_T^{-1}\|u-\Pi_T^{k+1}(u)\|_{\partial T^D}^2. \tag{7.23}$$

proof. As in Lemma 4.6, rearranging the terms, using the definition of the bilinear form a_T^ε, the definition of the lifting operator L_T^ε, the exact solution of the reaction diffusion equation, we have $\mathcal{D}_h^\varepsilon(\hat{v}_h^i) = \Psi_1^\varepsilon + \Psi_2^\varepsilon$ with

$$\begin{aligned}\Psi_1^\varepsilon = \sum_{T\in\mathcal{T}_h}\Big(&-(\varepsilon\nabla(\mathcal{E}(u)-u)\cdot\boldsymbol{n}_T, v_T^{k+1})_{\partial T^D} + (\mathcal{E}(u)-u, v_T^{k+1})_{T,\varepsilon} \\ &+ (\varepsilon\nabla(\mathcal{E}(u)-u)\cdot\boldsymbol{n}_T, v_{\partial T^i}^k - v_T^{k+1})_{\partial T^i}\Big), \\ \Psi_2^\varepsilon = \sum_{T\in\mathcal{T}_h}&\big(\sigma_T h_T^{-1}(\Pi_{\partial T^i}^k(u-\Pi_T^{k+1}(u)), v_{\partial T^i}^k - v_T^{k+1})_{\partial T^i} + \varepsilon h_T^{-1}(\Pi_T^{k+1}(u)-u, v_T^{k+1})_{\partial T^D}\big).\end{aligned}$$

Then, the Cauchy-Schwarz inequality and discrete trace inverse inequality finish this proof.

■

Lemma 7.6 (energy error estimate)**.** *Let $u \in H^{t+1}(\Omega)$, $t > \frac{1}{2}$ and $u|_T \in H^{k+2}(T)$ for all*

$T \in \mathcal{T}_h$ to be the solution of the problem (7.1)*, we have*

$$\sum_{T\in\mathcal{T}_h} \left(\|u - u_T^{k+1}\|_{T,\varepsilon}^2\right) \lesssim \sum_{T\in\mathcal{T}_h} \left(\sigma_T h_T^{2(k+1)} |v|_{H^{k+2}(T)}^2\right). \tag{7.24}$$

proof. As in Lemma 4.7, using the definition of $\mathcal{D}_h^\varepsilon$, we have $\mathcal{D}_h^\varepsilon(\hat{e}_h) = a_h^\varepsilon(\hat{e}_h, \hat{e}_h)$. The coercivity (Lemma 7.1) and consistency (Lemma 7.5) of a_h^ε shows

$$\|\hat{e}_h\|_{a_h^\varepsilon}^2 \lesssim a_h^\varepsilon(\hat{e}_h, \hat{e}_h) = \mathcal{D}_h(\hat{e}_h) \lesssim \sum_{T\in\mathcal{T}_h} \left(\|g_T^\varepsilon\|_{*T}^2 + \|\xi_T^\varepsilon\|_{\#T}^2\right)^{\frac{1}{2}} \times \|\hat{e}_h\|_{a_h^i}.$$

Since $u - u_T^{k+1} = (u - \Pi_T^{k+1}(u)) + e_T$, invoking the triangle inequality leads to $\sum_{T\in\mathcal{T}_h} \|u - u_T^{k+1}\|_{T,\varepsilon}^2 \lesssim \sum_{T\in\mathcal{T}_h} \left(\|u - \Pi_T^{k+1}(u)\|_{T,\varepsilon}^2 + \|g_T^\varepsilon\|_{*T}^2 + \|\xi_T^\varepsilon\|_{\#T}^2\right)$. Then, the approximation results (2.7) implies the result. ■

Lemma 7.7 (discrete energy error estimate)**.** *Let $u \in H^{t+1}(\Omega)$, $t > \frac{1}{2}$ and $u|_T \in H^{k+2}(T)$ for all $T \in \mathcal{T}_h$ to be the solution of the problem* (7.1) *and let $\hat{u}_h^i \in \hat{V}_h^i$ be the HHO-N solution. Then, we have*

$$\begin{aligned}\|\hat{e}_h\|_{a_h^\varepsilon}^2 &\lesssim \sum_{T\in\mathcal{T}_h} \left(\|R_h^\varepsilon(\hat{e}_h)\|_{T,\varepsilon}^2\right) + s_h^\varepsilon(\hat{e}_h, \hat{e}_h) \\ &\lesssim \Big(\sum_{T\in\mathcal{T}_h} \|g_T^\varepsilon\|_{*T}^2 + \|\xi_T^\varepsilon\|_{\#T}^2\Big) \lesssim \sum_{T\in\mathcal{T}_h} \left(\sigma_T h_T^{2(k+1)} |v|_{H^{k+2}(T)}^2\right).\end{aligned} \tag{7.25}$$

proof. We have $a_h^\varepsilon(\hat{e}_h, \hat{e}_h) = \mathcal{D}_h(\hat{e}_h)$. The stability (Lemma 4.1), approximation result (2.7) and Lemma 4.4 infer

$$\begin{aligned}\|\hat{e}_h\|_{a_h^i}^2 \lesssim a_h^\varepsilon(\hat{e}_h, \hat{e}_h) = \mathcal{D}_h(\hat{e}_h) &\lesssim \Big(\sum_{T\in\mathcal{T}_h} \|g_T^\varepsilon\|_{*T}^2 + \|\xi_T^\varepsilon\|_{\#T}^2\Big)^{\frac{1}{2}} \times \|\hat{e}_h\|_{a_h^\varepsilon} \\ &\lesssim \sum_{T\in\mathcal{T}_h} \left(\sigma_T h_T^{2(k+1)} |v|_{H^{k+2}(T)}^2\right)^{\frac{1}{2}} \times \|\hat{e}_h\|_{a_h^i}.\end{aligned}$$

■

Theorem 7.1 (energy error estimate for the reconstruction operator)**.** *Let $u \in H^{t+1}(\Omega)$,*

$t > \frac{1}{2}$ and $u|_T \in H^{k+2}(T)$ for all $T \in \mathcal{T}_h$ to be the solution of the problem (7.1)*, we have*

$$\sum_{T\in\mathcal{T}_h} \|u - R_T^\varepsilon(\hat{u}_h^i) - L_T^{k+1}(g_D)\|_{T,\varepsilon}^2 \lesssim \sum_{T\in\mathcal{T}_h} \big(\sigma_T h_T^{2(k+1)} |v|_{H^{k+2}(T)}^2\big). \tag{7.26}$$

proof. Noticing that $u - R_T^\varepsilon(\hat{u}_h^i) - L_T^{k+1}(g_D) = u - R_T^\varepsilon \circ \hat{I}_T^i(u) - L_T^{k+1}(g_D) + R_T^\varepsilon \circ \hat{I}_T^i(u) - R_T^\varepsilon(\hat{u}_h^i)$, and the definition of the energy projection (7.18) and Lemma 7.3 show

$$\begin{aligned}\sum_{T\in\mathcal{T}_h} \|u - R_T^\varepsilon(\hat{u}_h^i) - L_T^{k+1}(g_D)\|_{T,\varepsilon}^2 &\lesssim \sum_{T\in\mathcal{T}_h} \big(\|u - \mathcal{E}_T(u)\|_{T,\varepsilon}^2 + \|R_T^\varepsilon \circ \hat{I}_T^i(u) - R_T^\varepsilon(\hat{u}_h^i)\|_{T,\varepsilon}^2\big) \\ &\lesssim \sum_{T\in\mathcal{T}_h} \big(\|u - \mathcal{E}_T(u)\|_{T,\varepsilon}^2 + \|g_T^\varepsilon\|_{*T}^2 + \|\xi_T^\varepsilon\|_{\#T}^2\big).\end{aligned}$$

Then, using the approximation results (2.7), we derive the final error bound. ■

Remark 7.3 (Error estimate)**.** *In the case where $\varepsilon = l_\Omega^2$, with l_Ω^2 to be the length scale of the domain. Then, we have $\sigma_T \approx \mathcal{O}(l_\Omega^2)$, so the the error estimate* (7.26) *implies that*

$$\sum_{T\in\mathcal{T}_h} \|\nabla(u - R_T^\varepsilon(\hat{u}_h^i) - L_T^{k+1}(g_D))\|_T^2 \lesssim \sum_{T\in\mathcal{T}_h} \big(h_T^{2(k+1)} |v|_{H^{k+2}(T)}^2\big).$$

which corresponds to the error estimate obtained in Chapter 4 for the Poisson problem. Instead, in the case with $\varepsilon \leq h_T^2$ (including $\varepsilon = 0$), one has $\sigma_T \approx h_T^2$, the error estimate (7.26) *implies that*

$$\sum_{T\in\mathcal{T}_h} \|(u - R_T^\varepsilon(\hat{u}_h^i) - L_T^{k+1}(g_D))\|_T^2 \lesssim \sum_{T\in\mathcal{T}_h} \big(h_T^{2(k+2)} |v|_{H^{k+2}(T)}^2\big).$$

7.4. Experimental Examples

Two examples are tested for the convergence properties of the HHO-N method, for the first one, let the computational domain $\Omega := (0,1)^2$, $u = \sin(\pi x)\sin(\pi y) + x^5 + y^5$, the pure Dirichlet boundary condition is imposed. The triangular mesh is used in this example, the convergence rate is tested with polynomial order $k = 0, 1, 2$ and on 64, 256, 1024, 4096 cells. For the second one, let the computational domain be the circle domain with the complex boundary used in section 6.4, $u = (\sin(\pi x)\sin(\pi y))^2$, the mixed boundary condition is imposed such that, when $x \leq 0.5$, we impose the Dirichlet boundary condition,

and when $x > 0.5$, the Neumann boundary condition is imposed. The triangular mesh is used in this example, the convergence rate is tested with polynomial order $k = 0, 1, 2$ and on 661, 1045, 2642, 7184 cells. The convergence rates for energy norm $(\sum_{T\in\mathcal{T}_h} \big(\|u - R_T^\varepsilon(\hat{u}_h^i) - L_T^{k+1}(g_D)\|_{T,\varepsilon}^2\big))^{\frac{1}{2}}$ are listed in Table 10.3 and Table 10.4. These results exactly confirm Theorem 7.1 : When our mesh is finer and finer, the convergence rate decreases. When mesh is fine enough, σ_T becomes ε, so the diffusion term dominates the equation and the convergence rate gradually decreases from $k + 2$ to $k + 1$.

One example is tested for the physical oscillation. We define the domain Ω as a polygon embedded in $[0, 1] \times [-1, 0]$ to approximate the robot EVANGELION-01 from the anime *Neon Genesis Evangelion*, see Figure 10.3. And we take the forcing data $f = 1$ and the pure Dirichlet boundary condition $g_D = 0$, $\varepsilon = 10^{-2}, 10^{-5}$, with 5001 triangular cells and the polynomial order is $k = 1$. According to the property of the reaction diffusion equation, there should be a layer (the physical oscillation) near the boundary, and we do observe it, see Figures 10.11, 10.12.

8. Conclusions and Personal Review

In this report, we implemented and analysed the HHO methods employing the Nitsche's boundary penalty techniques for the Poisson problem and the singular perturbed reaction-diffusion equation.

One interesting future direction for the HHO method is to design the adaptive algorithm based on the posterior error analysis. Another direction is to do the L^2 error estimate for the non-convex domain problems. In that case, we know little about the regularity of the exact solution and we prefer to estimate the error by using the data from the right-hand side and the domain boundary instead of the regularity of the exact solution.

During this internship, my abilities in mathematics and programming have improved considerably. First of all, after these three months of training, my understanding of linear elliptic partial differential equations has been significantly improved. For example, I have a more intuitive and profound understanding of the regularity of the solution, and the effect of the regularity of the solution on the convergence rate of the numerical method, the influence of the regularity of boundary, etc. Since then, my understanding of numerical methods has also made great breakthroughs, such as the limitations of the continuous finite element method, the advantages of the discontinuous finite element method compared with it, and the excellent performance of the hybrid method in numerical aspects. Secondly, after three months of training, I am basically familiar with the theoretical analysis process of the HHO method, the general finite element method, and the usage of basic mathematical tools. The study of Nitsche's method strengthened my understanding of the concept of 'weakly imposed', while the study of the diffusion-reaction equation helped me to understand the advantages of Nitsche's method in dealing with such problems.

The entire internship process was basically carried out according to the original plan, but a lot of extra time was spent on some numerical experiments and several difficult theoretical analyses, so the time for writing the final report has been reduced to a certain extent. The most difficult part of the internship is debugging. Basically, every numerical example required two or three days of debugging. This is very torturous, but my programming ability has been significantly improved.

Due to the impact of the epidemic, I can freely choose whether to work remotely during the internship, but thanks to INRIA's air conditioning, I basically choose to work in the office every day, and my tutor is also in the office every day, so the efficiency of the entire internship is very considerable.

In terms of language, the communication with colleagues in the institute is basically English and French, so my foreign language proficiency has also been improved to a certain extent.

I have learned many research fields from my colleagues in INRIA, which include not only basic mathematics and applied mathematics, but also a lot of knowledge in finance and computers. This knowledge from different directions has enriched my knowledge reserve and deepened my understanding of mathematics from different perspectives. This knowledge has also helped me to find the career I want to do in the future and the field I hope to engage in. During the period of INRIA, I do feel that my understanding of partial differential equations has improved by a level compared with before. The discussion with my colleagues in convex optimization, finance, probability also gave me a more concrete understanding of the framework of mathematics, and I often feel that all fields are interoperable, and the research methods and theoretical skills in many fields can be used in other fields.

9. Conclusions et Bilan personnel

Dans ce rapport, nous avons mis en œuvre et analysé les méthodes HHO en utilisant les techniques de pénalité de Nitsche à la frontière pour le problème de Poisson et l'équation de réaction-diffusion singulièrement perturbée.

Une direction future intéressante pour la méthode HHO est de concevoir l'algorithme adaptatif basé sur l'analyse d'erreur a posteriori. Une autre direction consiste à faire l'estimation d'erreur L^2 pour les problèmes de domaine non convexe. Dans ce cas, nous savons peu de choses sur la régularité de la solution exacte et nous préférons estimer l'erreur en utilisant les données du force et des conditions aux limites, au lieu de la régularité de la solution exacte.

Au cours de ce stage, mes capacités en mathématiques et en programmation se sont considérablement améliorées. Tout d'abord, après ces trois mois de formation, ma compréhension des équations aux dérivées partielles elliptiques linéaires s'est considérablement accrue. Par exemple, j'ai une compréhension plus profonde de la régularité de la solution, et de l'influence de la régularité de la solution sur la performance de la méthode numérique, sur l'influence des conditions aux limites sur la régularité de la solution, etc. En outre, ma compréhension des méthodes numériques a également fait de grandes avancées, telles que les limitations de la méthode des éléments finis continus, les avantages de la méthode des éléments finis discontinus par rapport à celle-ci, et les excellentes performances des méthodes hybrides dans les solutions numériques. Deuxièmement, après trois mois de formation, je me suis fondamentalement familiarisé avec le processus d'analyse théorique de la méthode HHO et la méthode générale des éléments finis et l'utilisation des outils mathématiques fondamentaux. L'étude de la méthode de Nitsche a renforcé ma compréhension du concept de 'faiblement imposé', tandis que l'étude de l'équation de réaction-diffusion m'a aidé à comprendre concrètement les avantages de la méthode de

Nitsche pour traiter de tels problèmes.

L'ensemble du stage s'est essentiellement déroulé selon le plan initial. Beaucoup de temps a été consacré à certaines expériences numériques et à plusieurs points d'analyse théorique plus difficiles. La partie la plus ardue du stage a été le débogage. En effet, chaque exemple numérique a nécessité deux ou trois jours de débogage. Le fruit de mes efforts est que mes capacités de programmation ont été considérablement améliorées.

En raison de l'épidémie, j'avais pu librement choisir de travailler à distance pendant le stage. Mais il m'a été possible de travailler en présentiel et de rencontrer librement mon tuteur. Ainsi, l'efficacité de l'ensemble du stage a été très élevée.

En termes de langue, la communication avec les collègues de l'institut est essentiellement l'anglais et le français, donc ma maîtrise des langues étrangères s'est également améliorée dans une certaine mesure.

J'ai découvert de nombreux domaines de recherche auprès de mes collègues d'Inria, qui incluent non seulement les mathématiques fondamentales et les mathématiques appliquées, mais aussi beaucoup de connaissances en finance et en informatique. Ces connaissances provenant de différentes directions ont enrichi ma culture et approfondi ma compréhension des mathématiques sous différents angles. Ces connaissances m'ont également aidé à choisir le travail que je veux faire à l'avenir et le domaine dans lequel j'espère m'engager. J'espère m'engager dans la recherche sur les équations aux dérivées partielles dans le futur et ce stage m'en a donné l'envie. Durant la période d'Inria, j'ai senti que ma compréhension des équations aux dérivées partielles s'était significativement améliorée par rapport à avant, et la discussion avec mes collègues en optimisation convexe, finance, probabilités m'a également permis de mieux comprendre le cadre des mathématiques, et j'ai souvent l'impression que tous les domaines sont interopérables et que les méthodes de recherche et les compétences théoriques dans de nombreux domaines peuvent être utilisées dans d'autres domaines.

10. Appendix

All tables and figures are listed here.

10.1. Domains used in this report

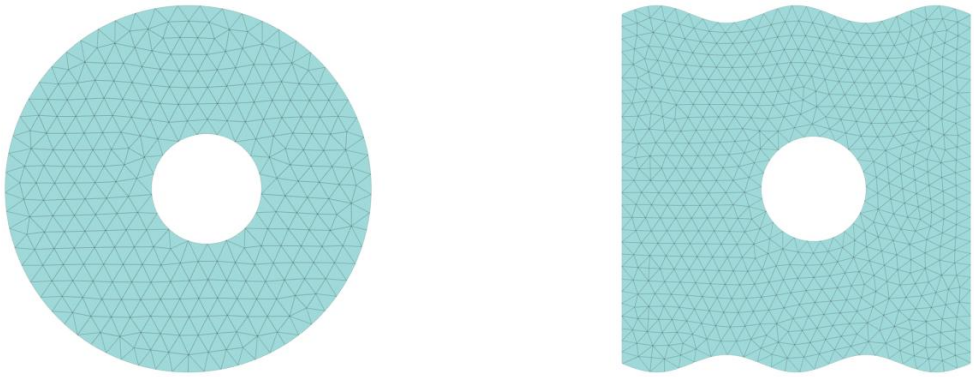

FIGURE 10.1 – Curved domains used in HHO-N method

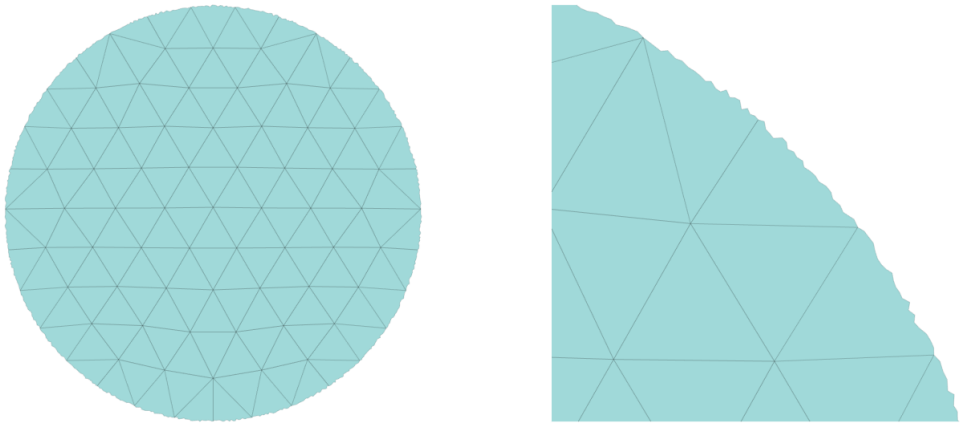

FIGURE 10.2 – Complex domain used in HHO-N method

FIGURE 10.3 – The image of EVANGELION-01 (left) and its approximated polygon domain (right)

10.2. Figures of section 6.1

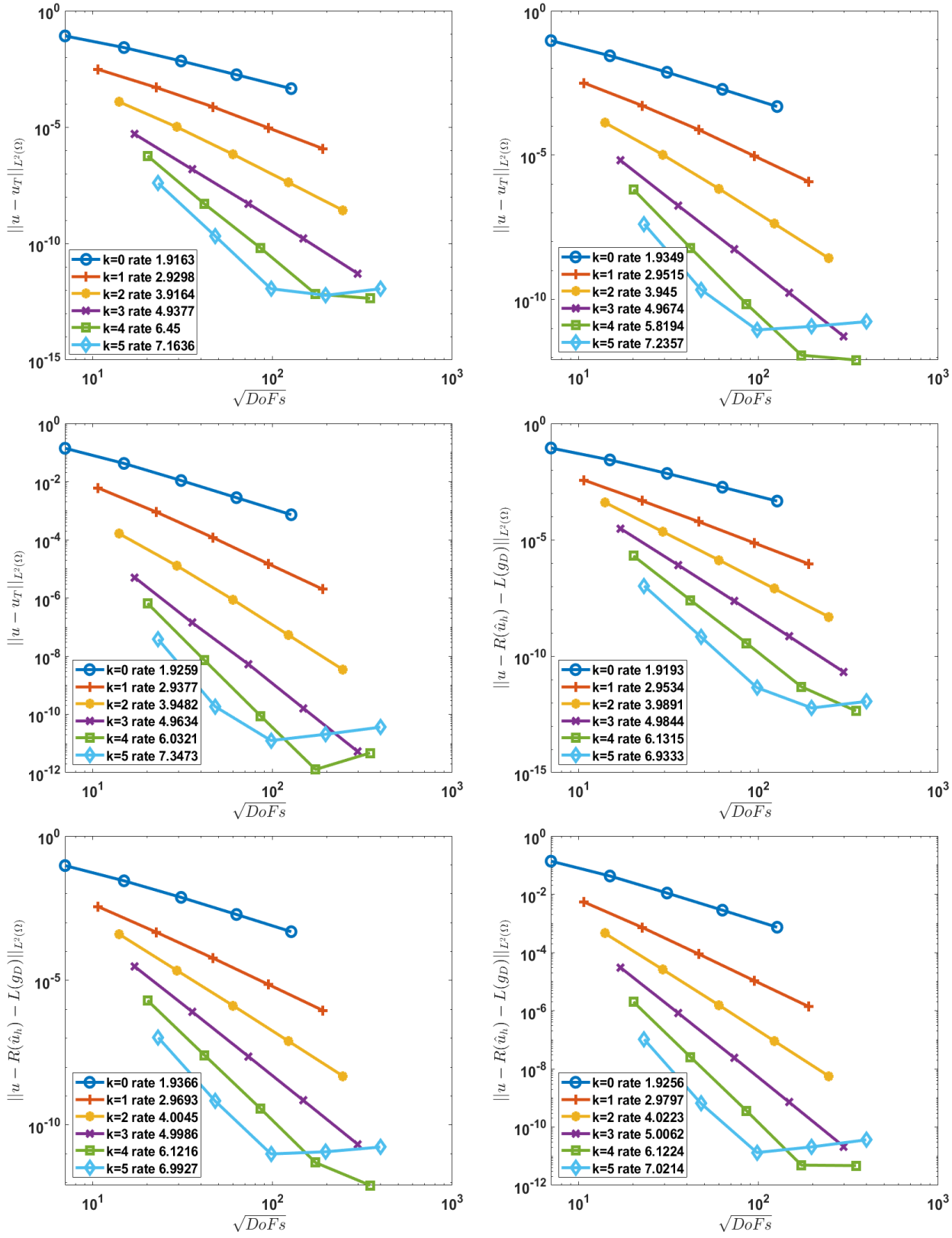

FIGURE 10.4 – Experimental convergence Rate of L^2 errors for equal-order HHO, mixed-order HHO and HHO-N respectively

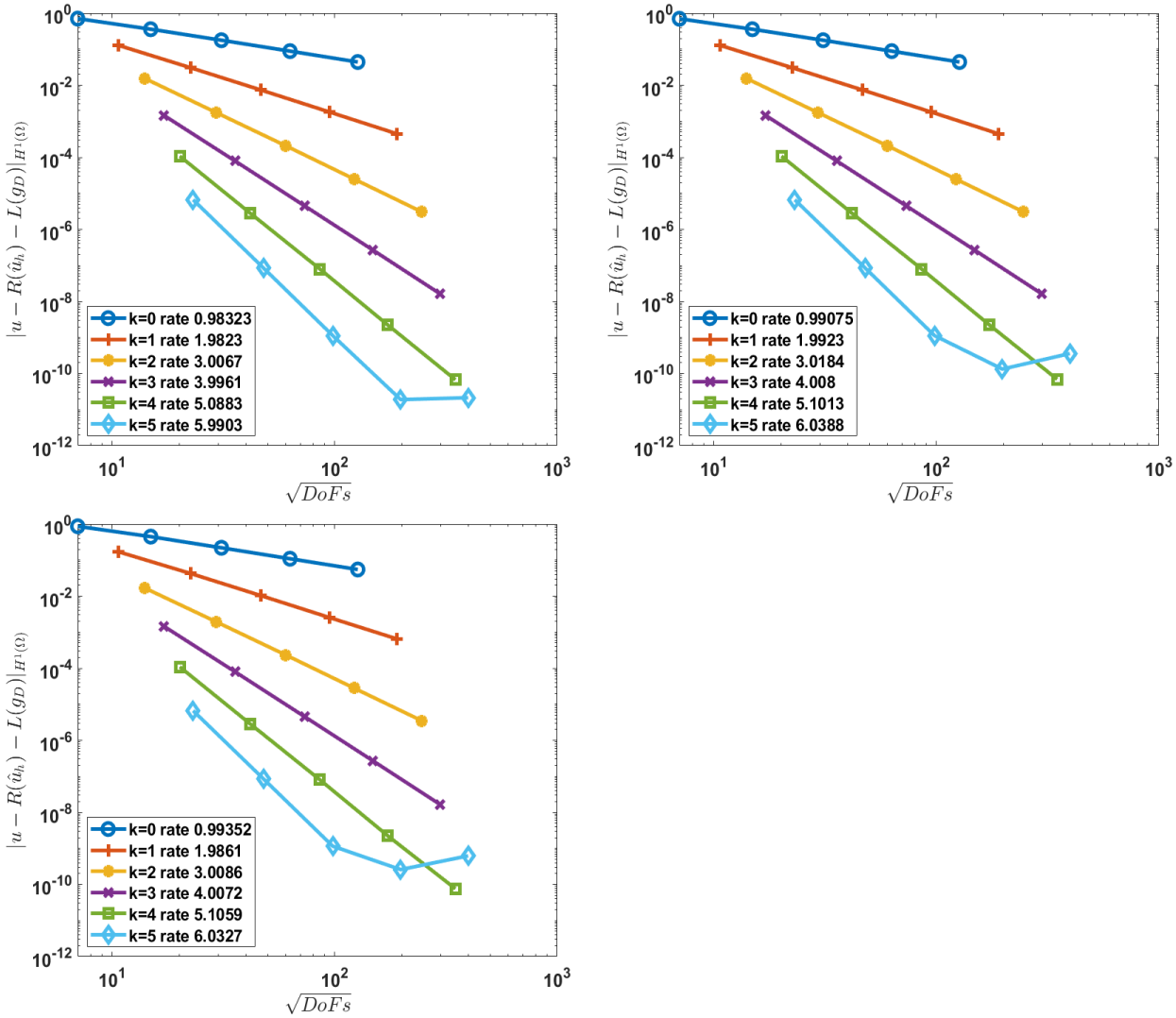

FIGURE 10.5 – Experimental convergence Rate of H^1 for equal-order HHO, mixed-order HHO and HHO-N respectively

10.3. Figures of section 6.2

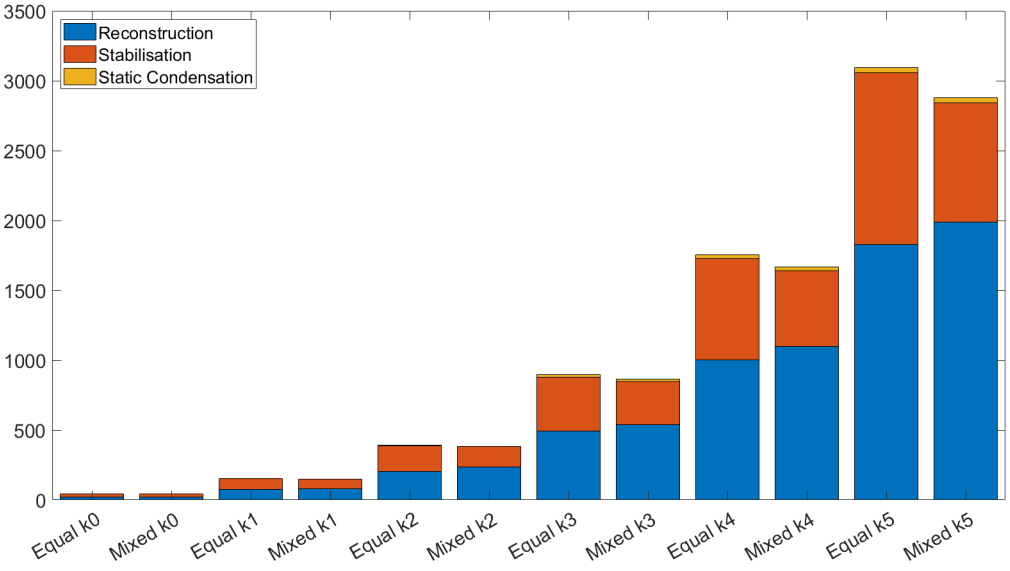

FIGURE 10.6 – The computational time of equal-order HHO and mixed-order HHO

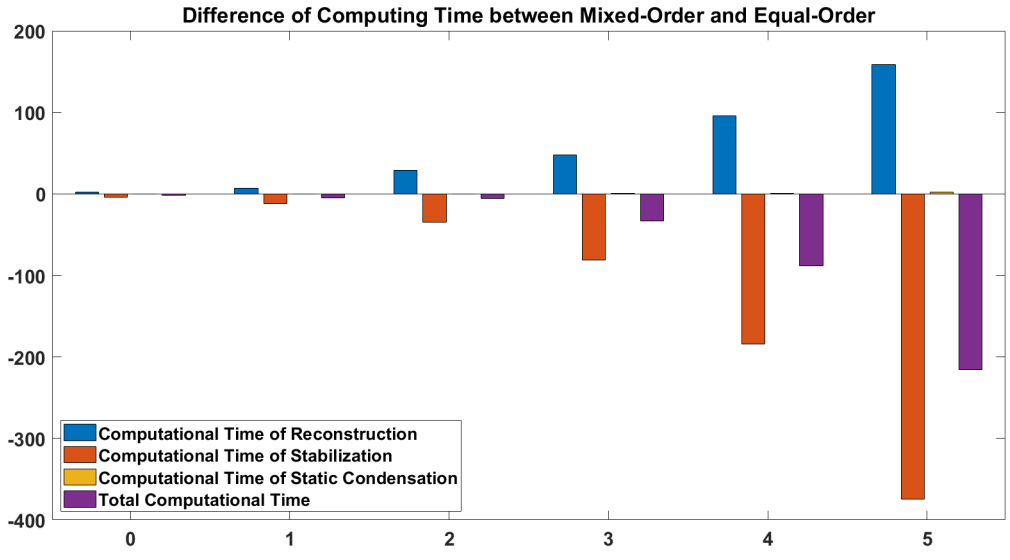

FIGURE 10.7 – The the difference of the mixed-order HHO and the equal-order HHO

10.4. Figures of section 6.3

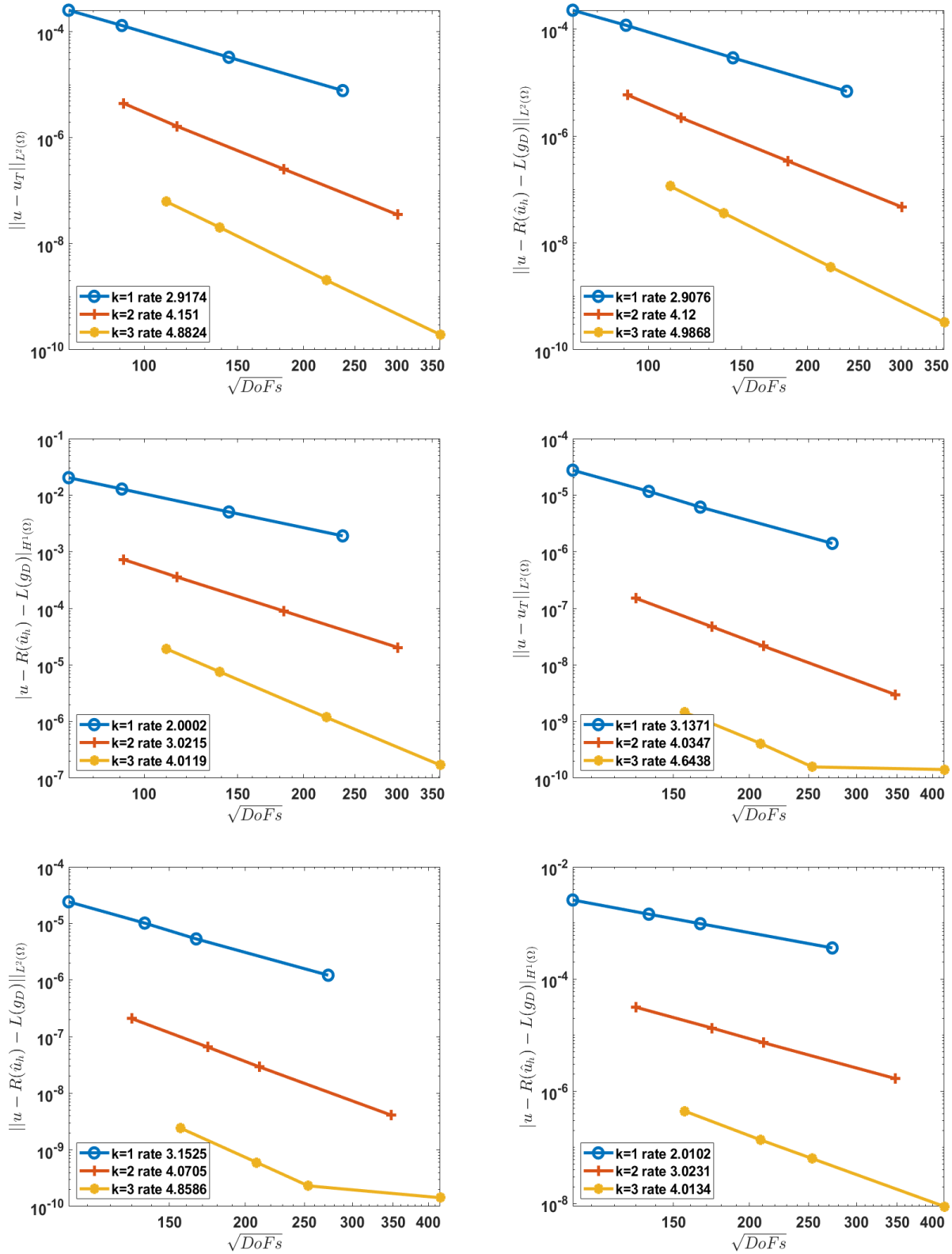

FIGURE 10.8 – Experimental convergence rate for curved domains : First three figures are for the circle with a hole, second three figures are for the waved rectangle with a hole

10.5. Figures of section 6.4

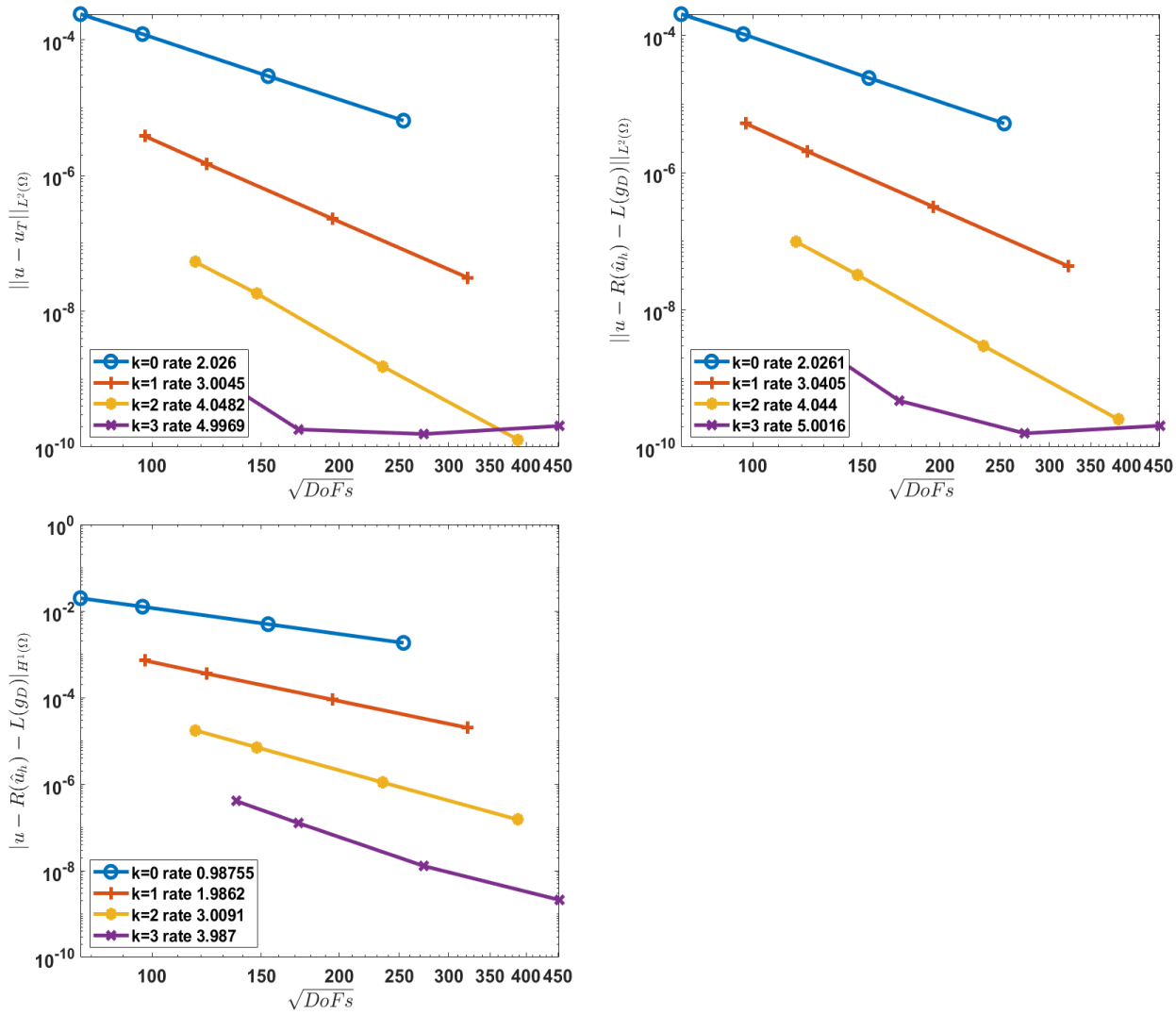

FIGURE 10.9 – Experimental convergence rate for a complex domain

10.6. Figures of section 6.5

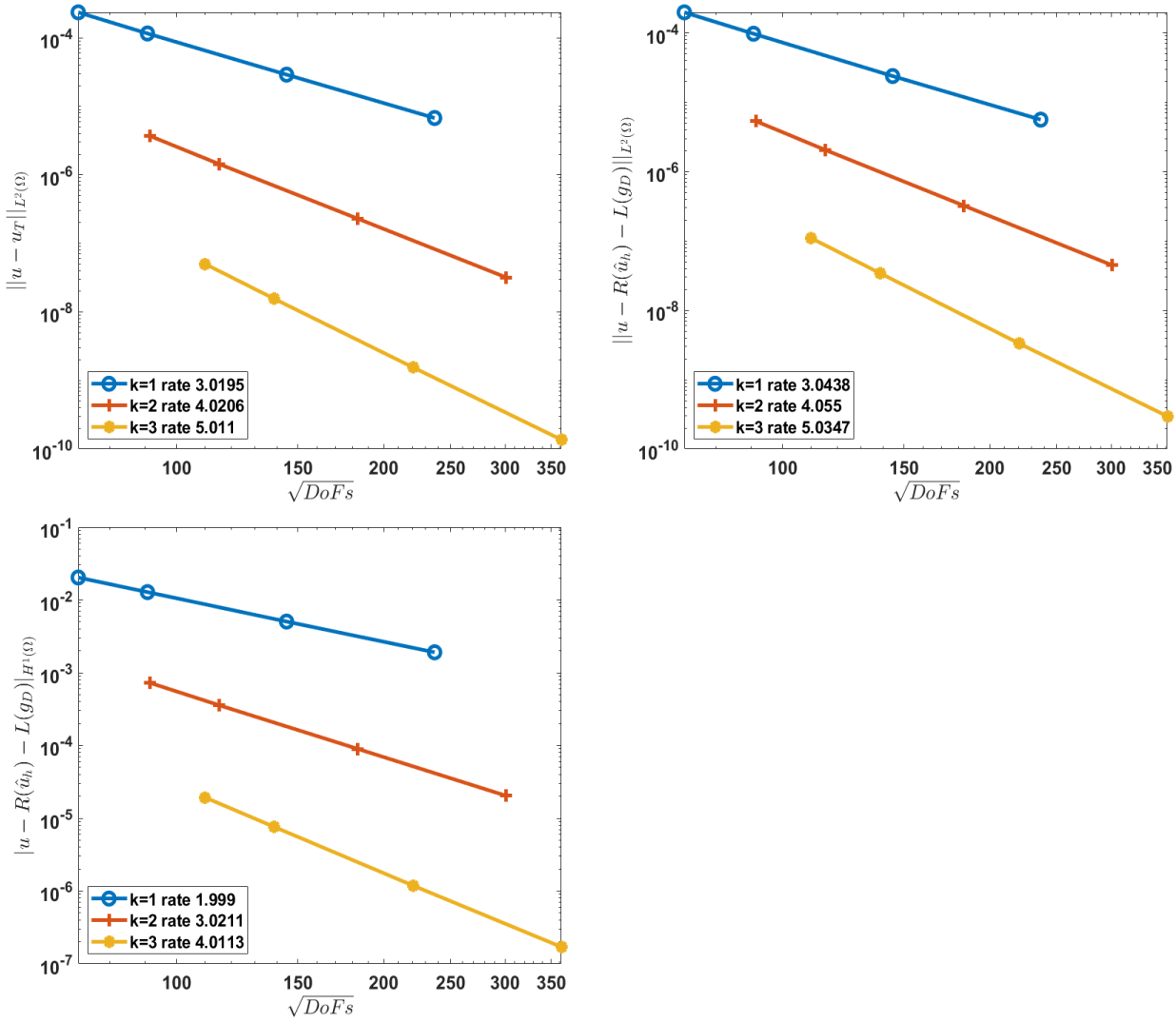

FIGURE 10.10 – Experimental convergence rate for curved domain With quasi-H^1 orthogonal basis

10.7. Tables of section 6.6

TABLE 10.1 – Condition number with Legendre basis

Cell \ order of face basis	1	2	3
584	8.51×10^2	1.86×10^3	3.06×10^3
925	1.37×10^3	2.98×10^3	4.82×10^3
2336	3.32×10^3	7.342×10^3	1.19×10^4
6272	9.13×10^3	2.01×10^4	3.25×10^4

TABLE 10.2 – Condition number with quasi-H^1 orthogonal basis

Cell \ order of face basis	1	2	3
584	5.77×10^2	1.01×10^3	1.35×10^3
925	9.48×10^2	1.59×10^3	2.11×10^3
2336	2.39×10^3	3.97×10^3	5.08×10^3
6272	6.78×10^3	1.10×10^4	1.41×10^4

10.8. Figures of chapter 7

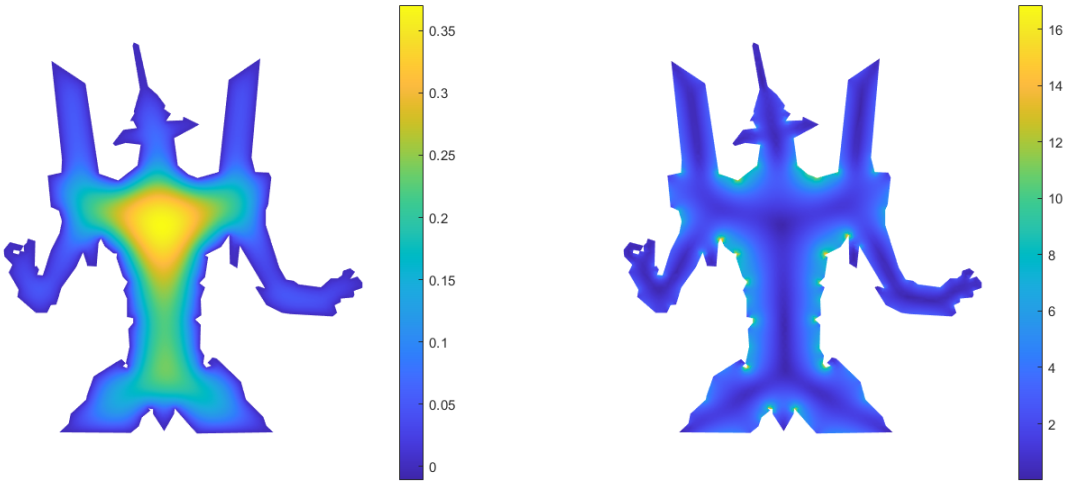

FIGURE 10.11 – The numerical solution of u (left) and the L^2 norm of its gradient (right) when $\varepsilon = 10^{-2}$

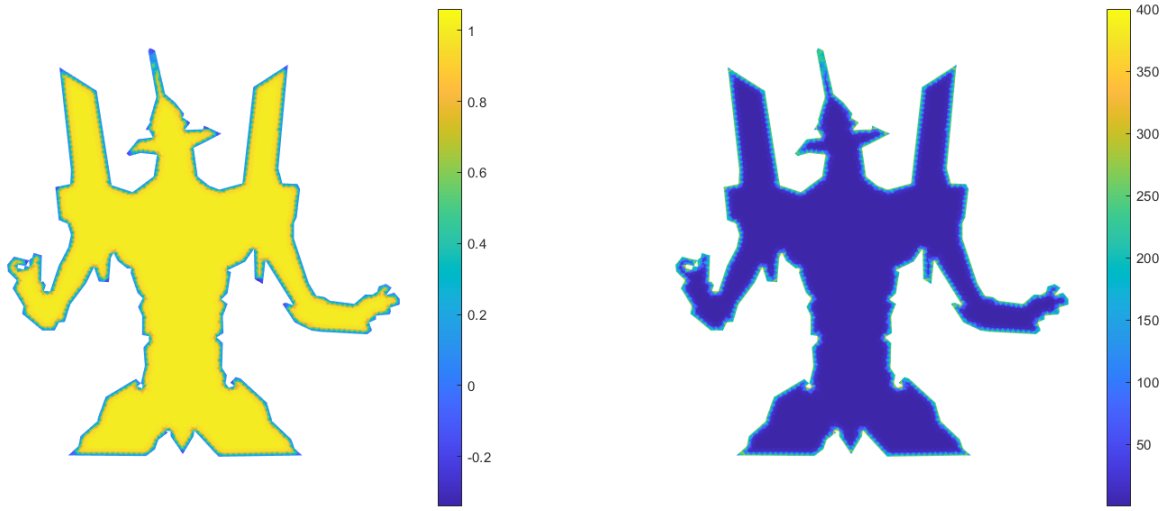

FIGURE 10.12 – The numerical solution of u (left) and the L^2 norm of its gradient (right) when $\varepsilon = 10^{-5}$

10.9. Tables of chapter 7

# Cell & rate	$\varepsilon = 1$	$\varepsilon = 10^{-3}$	$\varepsilon = 10^{-4}$	$\varepsilon = 10^{-5}$	$\varepsilon = 0$
		Rectangular domain with $k = 0$			
64	-	-	-	-	-
256	1.0007	1.0901	1.5282	1.8626	1.9256
1024	0.9793	1.0420	1.2166	1.7242	1.9388
4096	0.9822	1.0038	1.0730	1.4491	1.9687
		Rectangular domain with $k = 1$			
64	-	-	-	-	-
256	1.9238	2.2501	2.6704	2.7669	2.7778
1024	1.9091	2.0485	2.4724	2.8126	2.8616
4096	1.9294	1.7100	2.1784	2.7289	2.9442
		Rectangular domain with $k = 2$			
64	-	-	-	-	-
256	2.8607	3.0492	3.3570	3.6468	3.7104
1024	2.9014	3.1207	3.2026	3.6315	3.8391
4096	2.9391	2.9263	3.1800	3.4692	3.9707

TABLE 10.3 – Convergence rate of the HHO-N method in energy-norms for different k and ε in rectangle domain

# Cell & rate	$\varepsilon = 1$	$\varepsilon = 10^{-3}$	$\varepsilon = 10^{-4}$	$\varepsilon = 10^{-5}$	$\varepsilon = 0$
		Complex domain with $k = 0$			
661	-	-	-	-	-
1045	0.9902	0.8639	1.0360	1.8258	2.1002
2642	0.9899	0.9140	0.8705	1.5806	2.0437
7184	0.9936	0.9546	0.8280	1.2159	2.0165
		Complex domain with $k = 1$			
661	-	-	-	-	-
1045	2.0125	2.0724	2.3853	2.8927	3.0381
2642	2.0014	2.0684	2.2005	2.7154	2.9591
7184	1.9997	2.0559	2.0861	2.5320	3.0068
		Complex domain with $k = 2$			
661	-	-	-	-	-
1045	3.0158	3.0821	3.1841	3.7167	4.0532
2642	2.9821	3.0836	3.0733	3.4831	3.9949
7184	3.0020	3.1452	3.0622	3.2763	4.0232

TABLE 10.4 – Convergence rate of the HHO-N method in energy-norms for different k and ε in circle domain with complex boundary

References

[1] M. Abbas, A. Ern, and N. Pignet. A hybrid high-order method for incremental associative plasticity with small deformations. *Comput. Methods Appl. Mech. Engrg.*, 346 :891–912, 2019.

[2] J. Aghili, S. Boyaval, and D. A. Di Pietro. Hybridization of mixed high-order methods on general meshes and application to the stokes equations. *Comput. Methods Appl. Math.*, 2015.

[3] F. Bonaldi, D. A. Di Pietro, G. Geymonat, and F. Krasucki. A hybrid high-order method for kirchhoff–love plate bending problems. *ESAIM Math. Model. Numer. Anal.*, 52(2) :393–421, 2018 ;2017 ;.

[4] L. Botti and D. A. Di Pietro. Assessment of hybrid high-order methods on curved meshes and comparison with discontinuous Galerkin methods. *J. Comput. Phys.*, 370 :58–84, 2018.

[5] M. Botti, D. A. Di Pietro, and P. Sochala. A hybrid high-order method for nonlinear elasticity. *SIAM J. Numer. Anal.*, 55(6) :2687–2717, 2017.

[6] E. Burman, S. Claus, P. Hansbo, M. G. Larson, and A. Massing. Cutfem : Discretizing geometry and partial differential equations. *Internat. J. Numer. Methods Engrg.*, 104(7) :472–501, 2015.

[7] E. Burman, O. Duran, and A. Ern. Hybrid high-order methods for the acoustic wave equation in the time domain. *Commun. Appl. Math. Comput.*, pages 1–37, 2021.

[8] E. Burman and A. Ern. An unfitted hybrid high-order method for elliptic interface problems. *SIAM J. Numer. Anal.*, 56(3) :1525–1546, 2018.

[9] E. Burman and P. Hansbo. Fictitious domain finite element methods using cut elements : Ii. a stabilized nitsche method. *Appl. Numer. Math.*, 62(4) :328–341, 2012.

[10] A. Cangiani, Z. Dong, and E. H. Georgoulis. *hp*-version discontinuous Galerkin methods on essentially arbitrarily-shaped elements. *Math. Comp.*, 2021. Published online.

[11] K. L. Cascavita, F. Chouly, and A. Ern. Hybrid high-order discretizations combined with nitsche's method for dirichlet and signorini boundary conditions. *IMA J. Numer. Anal.*, 40(4) :2189–2226, 2020.

[12] M. Cicuttin, D. A. Di Pietro, and A. Ern. Implementation of discontinuous skeletal methods on arbitrary-dimensional, polytopal meshes using generic programming. *J. Comput. Appl. Math.*, 344 :852–874, 2018.

[13] M. Cicuttin, A. Ern, and T. Gudi. Hybrid high-order methods for the elliptic obstacle problem. *J. Sci. Comput.*, 83(1), 2020.

[14] M. Cicuttin, A. Ern, and N. Pignet. Hybrid high-order methods. a primer with application to solid mechanics. *to appear in Springer brief*, 2021.

[15] J. Dabaghi and G. Delay. A unified framework for high-order numerical discretizations of variational inequalities. *Comput. Math. Appl.*, 92 :62–75, 2021.

[16] D. A. Di Pietro, J. Droniou, and A. Ern. A discontinuous-skeletal method for advection-diffusion-reaction on general meshes. *SIAM J. Numer. Anal.*, 53(5) :2135–2157, 2015 ;2014 ;.

[17] D. A. Di Pietro and A. Ern. *Mathematical Aspects of Discontinuous Galerkin Methods*, volume 69. Springer Berlin Heidelberg, Berlin, Heidelberg, 2012.

[18] D. A. Di Pietro and A. Ern. A hybrid high-order locking-free method for linear elasticity on general meshes. *Comput. Methods Appl. Mech. Engrg.*, 283 :1–21, 2015.

[19] D. A. Di Pietro and A. Ern. Arbitrary-order mixed methods for heterogeneous anisotropic diffusion on general meshes. *IMA J. Numer. Anal.*, 37(1) :40–63, 2017.

[20] D. A. Di Pietro, A. Ern, and S. Lemaire. An arbitrary-order and compact-stencil discretization of diffusion on general meshes based on local reconstruction operators. *Comput. Methods Appl. Math.*, 14(4) :461–472, 2014.

[21] D. A. Di Pietro, A. Ern, A. Linke, and F. Schieweck. A discontinuous skeletal method for the viscosity-dependent stokes problem. *Comput. Methods Appl. Mech. Engrg.*, 306 :175–195, 2016.

[22] D. A. Di Pietro and S. Krell. A hybrid high-order method for the steady incompressible navier–stokes problem. *J. Sci. Comput.*, 74(3) :1677–1705, 2018 ;2016 ;.

[23] A. Ern and J.-L. Guermond. Finite element quasi-interpolation and best approximation. *ESAIM Math. Model. Numer. Anal. (M2AN)*, 51(4) :1367–1385, 2017.

[24] A. Ern and J.-L. Guermond. *Finite Elements II : Galerkin approximation, elliptic and mixed PDEs*. Springer, 2021.

[25] P. Grisvard. *Elliptic problems in nonsmooth domains*. Pitman Advanced Pub. Program, 1985.

[26] C. Lehrenfeld. Hybrid Discontinuous Galerkin Methods for Incompressible Flow Problems. Master's thesis, RWTH Aachen, May 2010.

[27] H. Roos, M. Stynes, and L. Tobiska. *Robust numerical methods for singularly perturbed differential equations*, volume 24 of *Springer Series in Computational Mathematics*. Springer-Verlag, Berlin, second edition, 2008. Convection-diffusion-reaction and flow problems.

[28] A. Veeser and R. Verfürth. Poincaré constants for finite element stars. *IMA J. Numer. Anal.*, 32(1) :30–47, 2012.

[29] H. Wu and Y. Xiao. An unfitted *hp*-interface penalty finite element method for elliptic interface problems. *J. Comput. Math.*, 37(3) :316–339, 2019.

[30] W. Zheng and H. Qi. On Friedrichs-Poincaré-type inequalities. *J. Math. Anal. Appl.*, 304(2) :542–551, 2005.